

CONSTRUCTION OF HIERARCHICALLY SEMI-SEPARABLE MATRIX REPRESENTATION USING ADAPTIVE JOHNSON–LINDENSTRAUSS SKETCHING*

YOTAM YANIV[†], OSMAN ASIF MALIK[‡], PIETER GHYSELS[‡], AND XIAOYE S. LI[‡]

Abstract. We extend an adaptive partially matrix-free Hierarchically Semi-Separable (HSS) matrix construction algorithm by Gorman et al. [SIAM J. Sci. Comput. 41(5), 2019] which uses Gaussian sketching operators to a broader class of Johnson–Lindenstrauss (JL) sketching operators. We present theoretical work which justifies this extension. In particular, we extend the earlier concentration bounds to all JL sketching operators and examine this bound for specific classes of such operators including the original Gaussian sketching operators, subsampled randomized Hadamard transform (SRHT) and the sparse Johnson–Lindenstrauss transform (SJLT). We discuss the implementation details of applying SJLT efficiently and demonstrate experimentally that using SJLT instead of Gaussian sketching operators leads to 1.5–2.5× speedups of the HSS construction implementation in the STRUMPACK C++ library. The generalized algorithm allows users to select their own JL sketching operators with theoretical lower bounds on the size of the operators which may lead to faster run time with similar HSS construction accuracy.

1. Introduction. Many large dense matrices in engineering and data sciences are *data-sparse* in that the off-diagonal blocks can be well approximated as low-rank submatrices. Some examples are matrices from discretized integral equations, boundary element methods, and kernel matrices used in statistical and machine learning [5, 8]. There are many types of matrix formats that can take advantage of the off-diagonal low-rank structure; these include, to name a few, Hierarchically Semi-Separable matrices (HSS) [6, 7], Hierarchical matrices (\mathcal{H}) and Hierarchical Bases \mathcal{H} -matrices (\mathcal{H}^2) [15, 14]. This work focuses on HSS representation and, more specifically, efficient HSS compression, i.e., construction of the HSS format. Compression is the central component of the HSS framework, and usually dominates the total cost. Once a matrix is compressed into its HSS form, one can develop asymptotically faster algorithms for multiplication, factorization and solve based on the HSS structure, and hence solve the algebraic equations efficiently. One way to speed up the HSS compression algorithm is to use randomization [22, 16], in particular, randomized sketching. The main advantage of randomization is that these methods usually require fewer floating point operations and less communication than their traditional deterministic counterparts. Moreover, they are often easier to parallelize.

Consider a matrix $A \in \mathbb{C}^{n \times n}$ to be compressed as an HSS matrix that approximates A . Randomized sketching can be considered as a preprocessing step that helps compute the column spaces of various off-diagonal submatrices throughout the compression algorithm. This preprocessing step is done by post-multiplying A by a

*Submitted to the editors DATE.

Funding: This research was supported by the Exascale Computing Project (17-SC-20-SC), a collaborative effort of the U.S. Department of Energy Office of Science and the National Nuclear Security Administration. This research used resources of the National Energy Research Scientific Computing Center (NERSC), a U.S. Department of Energy Office of Science User Facility located at Lawrence Berkeley National Laboratory, operated under Contract No. DE-AC02-05CH11231 using NERSC award ASCR-ERCAP0017690. YY was partially supported by the NSF MSGI summer internship program. OAM was supported by the U.S. Department of Energy, Office of Science, Office of Advanced Scientific Computing Research under Award Number DE-AC02-05CH11231. All opinions expressed in this paper are the author’s and do not necessarily reflect the policies and views of NSF, ORAU/ORISE, or DOE.

[†]University of California Los Angeles Department of Mathematics yotamya@math.ucla.edu.

[‡]Lawrence Berkeley National Laboratory {oamalik, pghysels, xsli}@lbl.gov.

tall-and-skinny random matrix R^T of size $n \times (r+p)$: $S \leftarrow AR^T$. If A is nonsymmetric, the row space must be computed separately which requires an additional preprocessing step of the form $S' \leftarrow A^*R^T$. The coefficient r is an upper bound on the ranks of the off-diagonal blocks and p is an oversampling parameter, a small integer on the order of 10 or so. The entries of the $n \times (r+p)$ matrix R^T are drawn from a certain probability distribution. A common choice is to draw the entries of R^T independently from an appropriately scaled normal distribution. The cost of matrix multiplication AR^T is $O(n^2d)$, where $d = r+p$ while the remaining cost of the compression algorithm is $O(nr^2)$, therefore this upfront matrix multiplication is often the bottleneck in the entire compression algorithm.

This paper builds upon our previous work [11, 13]. The first motivation is to mitigate the $O(n^2d)$ cost in the sketching step. To this end, we study alternative random sketching operators, including structured sketches like the sparse Johnson–Lindenstrauss transform (SJLT) [19] and the subsampled randomized Hadamard transform (SRHT) [1]. They are asymptotically faster to apply than Gaussian sketching operators, but research is needed to understand whether they provide desired approximation quality, and what the time and accuracy trade offs are. Secondly, one of the highlights of [13] is the development of a new stopping criterion for adaptive sketching, which is needed because the HSS rank r is usually not known *a priori*. Adaptivity ensures that we generate sufficient (for robustness), yet not too many (for high performance), random sketching operators (columns of R^T) until the range of A is well approximated. The stopping criterion in [13] is based on a probabilistic Frobenius norm estimation of A by the sketch matrix $S = AR^T$ and concentration bounds when sketching with Gaussian sketching operators. This analysis leads to a robust stopping criterion taking into account both absolute and relative errors. In this paper, we present theoretical analysis which justifies more general JL sketching operators. We extend the concentration bounds discussed in [13] to all real JL sketching operators and examine this bound for specific classes of JL sketching operators including the original Gaussian sketching operators, the SJLT, and the SRHT.

Remark 1.1. In most literature on randomized sketching, the sketching operator R is applied on the left of a vector or a matrix, such as RA . But in the HSS construction, we need to apply R on the right of A to probe its column space. Therefore, in the HSS context, we use the transpose notation AR^T , so we can readily apply the existing JL theory when appropriate.

The contributions of this work are:

- Gorman et al. [13] presented an adaptive HSS compression algorithm that requires Gaussian sketching operators. We generalize this algorithm to use any Johnson–Lindenstrauss (JL) sketching operators.
- We prove a range-finder bound for JL sketching operators and Sparse Johnson–Lindenstrauss Transforms (SJLT) which states that the sketch $S = AR^T$ for a low rank matrix A contains relevant range information of the original matrix. This allows us to use the sketch instead of the original block when doing HSS compression.
- We show that the Frobenius norm stopping criteria from Gorman et al. [13] are still valid for JL sketching operators and prove Frobenius norm bounds for JL sketching operators and SJLT.
- We implement our general HSS compression algorithm in the STRUMPACK C++ library [26] which allows the user to choose among sketching operators implemented in STRUMPACK or implement their own. We implement SJLT

as a specific use case and discuss the implementation details for SJLT in which we leverage a special data structure and multiplication routines for computing AR^T and A^*R^T .

- We compare our method using SJLT and the existing Gaussian sketching operators and observe $1.5\text{--}2.5\times$ speedups when using SJLT while maintaining the similar compression accuracy. The number of flops is reduced from $O(n^2d)$ to $O(n\alpha d)$, where $\alpha \ll d$; usually $\alpha = 2$ to 4 is sufficient.

The rest of the paper is organized as follows. In the end of this section we outline the notation for the rest of the paper. In [section 2](#) we discuss the background on HSS matrices, our HSS compression algorithm, [Algorithm 1](#), which we generalize from [\[13\]](#) and the Johnson–Lindenstrauss sketching operators which we use in our generalization. Next, in [section 3](#) we state and prove range-finder bound theory which is required to use Johnson–Lindenstrauss sketching operators as part of the HSS compression. Following [section 3](#), in [section 4](#) we discuss the adaptive stopping criteria in [Algorithm 1](#) which leverage a Frobenius norm stopping criteria. Then in [section 5](#) we prove that the Frobenius norm stopping criteria generalize to all Johnson–Lindenstrauss sketching operators. [Section 6](#) discusses the implementation details of using SJLT. Afterwards, in [section 7](#) we conduct experiments comparing SJLT and Gaussian sketching showing similar compression errors and faster compression when using SJLT. Finally, in [section 8](#) we state our concluding remarks.

1.1. Notation. Throughout this paper we denote a matrix as $A \in \mathbb{C}^{m \times n}$ unless otherwise stated. We let a random *sketching operator* be denoted as $R^T \in \mathbb{R}^{n \times d}$ and vectors $x \in \mathbb{R}^n$. We refer to $S = AR^T$ as a *sketch* of the matrix A . Sketching is the process of applying R^T to A on the right, computing AR^T . We use \log to represent the logarithm with base e . We let $\|A\|$, $\|x\|$ be the matrix and vector two-norm respectively. We let $\|A\|_F$ represent the Frobenius norm of a matrix. We define $[n] = (1:n) = \{1, \dots, n\}$ to be the set of integers from one to n . To represent indexing a row, column or sub-block of our matrix we use MATLAB notation. Where lower case i , j represent individual entries and upper case I , J represent index sets. For example $A(i, j)$ is entry (i, j) of matrix A , $A(i, :)$ is row i of matrix A and $A(I, J)$ is the sub-block of A containing the rows in index set I and columns in index set J . In the theory section to compress this notation we use $A_{i\cdot}$ to represent the row i of matrix A and $A_{\cdot j}$ to represent column j of matrix A . When computing a QR factorization for a matrix A we let $A = Q\Omega$ where Q is an orthogonal matrix and Ω is upper triangular. An interpolative decomposition of a matrix A with rank r is computed as $A = A(:, J)U$ where J is an index set of size r and U is an $r \times n$ matrix containing an $r \times r$ identity block. Finally, the projection operator onto a matrix S is defined as $P_S = SS^\dagger$.

2. Preliminaries. We begin this section by describing the HSS matrix format and the adaptive HSS construction algorithm. Then we discuss the relevant background to incorporate a more generalized and possibly faster randomization via Johnson–Lindenstrauss sketching in our HSS construction algorithm.

2.1. Background on HSS Matrices. Consider a square matrix $A \in \mathbb{C}^{n \times n}$ and index set $I_A = \{1, \dots, n\}$. The HSS matrix representation is a hierarchical block 2×2 partitioning of the matrix, where all off-diagonal blocks are compressed, or approximated, using a low-rank product, see [Figure 1a](#). The hierarchical structure is succinctly described by a binary tree \mathcal{T} , called *cluster tree*, as depicted in [Figure 1b](#). The recursive partitioning stops at the leaf level, which corresponds to the smallest

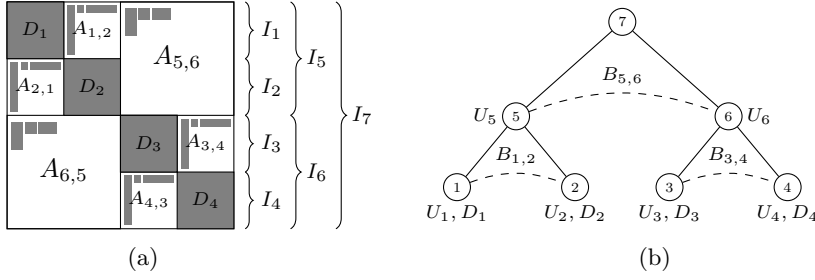


Fig. 1: (a) Illustration of a symmetric HSS matrix using 3 levels. Diagonal blocks are partitioned recursively. Gray blocks denote the basis matrices. (b) Tree for the HSS matrix from (a), using topological ordering. All nodes except the root store U_i (and V_i for the non-symmetric case). Leaves store D_i , non-leaves B_{ij} (and B_{ji} for the non-symmetric case).

block size of the partition. The leaves do not need to be of uniform size, because for certain input matrices a non-uniform partition may be preferable for better compression.

Each node $\tau \in \mathcal{T}$ is associated with a contiguous subset $I_\tau \subset I_{\text{root}(\mathcal{T})}$. We use $\#I_\tau$ to denote the cardinality of I_τ . For two children ν_1 and ν_2 of τ , it holds that $I_{\nu_1} \cup I_{\nu_2} = I_\tau$ and $I_{\nu_1} \cap I_{\nu_2} = \emptyset$. It follows that $\cup_{\tau \in \text{leaves}(\mathcal{T})} I_\tau = I_{\text{root}(\mathcal{T})} = I_A$. The same tree \mathcal{T} is used for the rows and the columns of A . Commonly, the tree nodes are numbered in a *postorder*, and most of the HSS algorithms, such as construction, matrix-vector multiplication, factorization and solve etc., can be described as traversing the cluster tree following this postorder. However, in the parallel implementation and throughout this paper, we traverse the cluster tree following a bottom-up *topological order*, i.e., from the leaf level to the root, level by level, displayed in [Figure 1b](#).

Each leaf node τ of \mathcal{T} corresponds to a diagonal blocks of A , denoted as D_τ , and is stored as a dense matrix: $D_\tau = A(I_\tau, I_\tau)$. At each node τ , the off-diagonal block $A(I_\tau, I_A \setminus I_\tau)$ is called a row *Hankel block*, and the off-diagonal block $A(I_A \setminus I_\tau, I_\tau)$ is a column Hankel block. The compression algorithm sweeps through the tree bottom-up. At each tree node, it computes the column basis for the row Hankel block and row basis for the column Hankel block. Note that all the blocks within a row (column) Hankel block share the same column (row) basis. The HSS algorithm goes further to reduce complexity: each internal node recycles the bases computed at the two children nodes, thus, the basis at each internal node has the nested structure (see Equation (2.2)), called *nested basis property*, which we describe now. For a node τ with two children ν_1 and ν_2 , the off-diagonal block $A_{\nu_1, \nu_2} = A(I_{\nu_1}, I_{\nu_2})$ is factored (approximately) as

$$(2.1) \quad A_{\nu_1, \nu_2} \approx U_{\nu_1}^{\text{big}} B_{\nu_1, \nu_2} (V_{\nu_2}^{\text{big}})^*,$$

where $U_{\nu_1}^{\text{big}}$ has dimensions $\#I_{\nu_1} \times r_{\nu_1}^r$, B_{ν_1, ν_2} is a submatrix of A_{ν_1, ν_2} with dimensions $\#I_{\nu_1} \times \#I_{\nu_2}$ and $V_{\nu_2}^{\text{big}}$ has dimensions $\#I_{\nu_2} \times r_{\nu_2}^c$ ¹. The *HSS-rank* r is defined as the maximum of r_τ^r and r_τ^c over all off-diagonal blocks, where typically $r \ll N$. B_{ν_1, ν_2}

¹Superscripts r and c are used to denote that $U^{\text{big}}/V^{\text{big}}$ are column/row bases for the row/column Hankel blocks of A .

Remark 2.1. In practice, the interpolative decomposition is computed using a rank revealing QR factorization as $A = A(:, J)V$ which computes a column basis. To compute a row basis, we compute the interpolative decomposition of $A^* = A^*(:, J)V$ and apply the conjugate transpose so $A = V^*A(J, :)$, then we can rename $V^* = U$ so $A = UA(J, :)$ resulting in a row basis.

We can represent a low rank matrix or Hankel block in our case as a basis matrix U and a sampling of the rows. Once we compute an interpolative decomposition for both Hankel row block and Hankel column block that intersect a low rank off diagonal HSS block we can combine the bases and the selected row and column samplings to create a low rank approximation. By leveraging the interpolative decomposition to do our local compression we recover an approximate basis for the Hankel block and a sampling of the most important r rows of our sketch. The r rows of the sketch correspond to r rows of the original matrix A , allowing us to only use our sketch to compress the Hankel blocks as long as **the sketch of the Hankel block is representative of the original Hankel block.**

In most practical problems, the HSS rank, rank of the low dimensional off diagonal blocks, is not known *a priori*, hence, the size of the sketching operator needs to be chosen adaptively. Previously, Gorman et al. [13] developed a *blocked incrementing strategy* which fully reuses the already-computed basis set in two ways: (1) at each HSS tree node τ , if the initial samples are not sufficient, we increase a block of samples Δd , and augment τ 's orthogonal basis by this amount; (2) This augmented basis will cause basis sets of the ancestor nodes to have sizes at least as large as that of τ , while the basis sets of the descendant nodes are not affected. [Algorithm 1](#) illustrates the high level HSS compression procedure with adaptation built in. The algorithm traverses the cluster tree in a topological order bottom-up. Initially each node τ is assigned the UNTOUCHED state. At the time when a node τ is to be compressed, all its descendant nodes are already COMPRESSED, and all its ancestral nodes are UNTOUCHED. Line 27 tests to see whether the sketch for τ is sufficiently representative. If so, τ is compressed and its state is changed to COMPRESSED. If not, in lines 35-37 of the else-branch, we extend the sketching operator by Δd columns, change τ 's state to PARTIALLY_COMPRESSED, and traverse the tree again with the following actions: (1) for the nodes below τ , we only subtract the newly added sketch from the diagonal blocks (lines 18 and 20); (2) for the current PARTIALLY_COMPRESSED node τ , we augment the already-computed basis set with the new Δd columns from the sketch (lines 29-30); (3) for τ 's ancestral nodes, compression proceeds with the entire sketch (line 23).

In the original adaptive compression algorithm from [13] the global sketch of the matrix A was computed using a Gaussian sketching operator. This sketching operator is dense so it requires $O(n^2)$ time to compute an additional column when trying to expand the sketch. In this paper, we extend the algorithm to any Johnson–Lindenstrauss sketching operator and use the sparse JL sketching operators, which can be applied faster, as a case study to show that we can speed up HSS compression by leveraging a sparse sketching operator. Additionally, our theory generalizes to a broader class of sketching operators some of which could be better suited for specific

applications with similar time complexity guarantees.

Algorithm 1: Adaptive HSS compression of $A \in \mathbb{C}^{n \times n}$ using cluster tree \mathcal{T} with relative and absolute tolerances ε_{rel} and ε_{abs} respectively, see [Table 1](#) for helper function details.

```

1 function  $H = \text{HSSCompressAdaptive}(A, \mathcal{T}, d_0, \Delta d)$ 
2    $d \leftarrow d_0$ ;  $n \leftarrow \text{cols}(A)$ 
3    $R \leftarrow \text{JL-Operator}(d + \Delta d, n)$ 
4    $S \leftarrow AR^T$ 
5   foreach  $\tau \in \mathcal{T}$  do  $\tau.\text{state} \leftarrow \text{UNTOUCHED}$ 
6   while  $\text{root}(\mathcal{T}).\text{state} \neq \text{COMPRESSED}$  and  $d < d_{\text{max}}$  do
7     foreach  $\tau \in \mathcal{T}$  in topological order do
8       if  $\tau.\text{state} = \text{UNTOUCHED}$  then
9         if  $\text{isleaf}(\tau)$  then  $D_\tau \leftarrow A(I_\tau, I_\tau)$ 
10        else
11           $\nu_1, \nu_2 \leftarrow \text{children}(\tau)$ 
12           $B_\tau \leftarrow A(\tilde{I}_{\nu_1}, \tilde{I}_{\nu_2})$ 
13           $\iota \leftarrow 1 : d + \Delta d$ 
14        else  $\iota \leftarrow d + 1 : d + \Delta d$ 
15        if  $\text{isroot}(\tau)$  then
16           $\tau.\text{state} \leftarrow \text{COMPRESSED}$ 
17          break
18        if  $\text{isleaf}(\tau)$  then  $S_\tau(:, \iota) \leftarrow S(I_\tau, \iota) - D_\tau R^T(I_\tau, \iota)$ 
19        else
20           $S_\tau(:, \iota) \leftarrow \begin{bmatrix} S_{\nu_1}(J_{\nu_1}, \iota) - B_\tau R_{\nu_2}(:, \iota) \\ S_{\nu_2}(J_{\nu_2}, \iota) - B_\tau^* R_{\nu_1}(:, \iota) \end{bmatrix}$ 
21        if  $\tau.\text{state} \neq \text{COMPRESSED}$  then
22          if  $\tau.\text{state} = \text{UNTOUCHED}$  then
23             $\{Q_\tau, \Omega_\tau\} \leftarrow \text{QR}(S_\tau(:, 1 : d))$ 
24             $\tilde{S} \leftarrow S_\tau(:, d + 1 : d + \Delta d)$  // last  $\Delta d$  columns
25             $\hat{S} \leftarrow (I - Q_\tau Q_\tau^*) \tilde{S}$ 
26             $\varepsilon_{\text{abs}}^\tau \leftarrow \varepsilon_{\text{abs}} / \text{level}(\tau)$ ;  $\varepsilon_{\text{rel}}^\tau \leftarrow \varepsilon_{\text{rel}} / \text{level}(\tau)$ 
27            if  $\|\hat{S}\|_F < \varepsilon_{\text{abs}}^\tau$  or  $\|\hat{S}\|_F < \varepsilon_{\text{rel}}^\tau \|\tilde{S}\|_F$  then // Eq. 4.1
28              goto line 32
29             $\{\hat{Q}, \hat{\Omega}\} \leftarrow \text{QR}(\hat{S})$ 
30             $Q_\tau \leftarrow \begin{bmatrix} Q_\tau & \hat{Q} \end{bmatrix}$ 
31            if  $\min(\text{diag}(|\hat{\Omega}|)) < \varepsilon_{\text{abs}}^\tau$  or  $\min(\text{diag}(|\hat{\Omega}|)) < \varepsilon_{\text{rel}}^\tau |\Omega_\tau|_{11}$  // Eq. 4.2
32              then
33                 $\{U_\tau^*, J_\tau\} \leftarrow \text{ID}(S_\tau^*, \varepsilon_{\text{rel}}^\tau, \varepsilon_{\text{abs}}^\tau)$ 
34                 $\tau.\text{state} \leftarrow \text{COMPRESSED}$ 
35              else
36                 $\bar{R} \leftarrow \text{JL-Operator}(\Delta d, n)$  // extending sketch
37                 $d \leftarrow d + \Delta d$ ;  $S \leftarrow [S \quad A\bar{R}^T]$ ;  $R^T \leftarrow [R^T \quad \bar{R}^T]$ 
38                 $\tau.\text{state} \leftarrow \text{PARTIALLY\_COMPRESSED}$ 
39                break
40            if  $\text{isleaf}(\tau)$  then
41               $R_\tau(:, \iota) \leftarrow U_\tau^* R^T(I_\tau, \iota)$ ;  $\tilde{I}_\tau \leftarrow I_\tau(J_\tau)$ 
42            else
43               $R_\tau(:, \iota) \leftarrow U_\tau^* \begin{bmatrix} R_{\nu_1}(:, \iota) \\ R_{\nu_2}(:, \iota) \end{bmatrix}$ ;  $\tilde{I}_\tau \leftarrow [I_{\nu_1} \quad I_{\nu_2}](J_\tau)$ 
44          end
45        end
46      end
47    end
48  end
49  return  $\mathcal{T}$ 

```

<code>cols(A)</code>	number of columns in matrix A
<code>JL-Operator(d, n)</code>	a $d \times N$ matrix drawn from a JL Distribution
<code>isleaf(τ)</code>	true if τ is a leaf node, false otherwise
<code>children(τ)</code>	a list with the children of node τ , always zero or two
<code>isroot(τ)</code>	true if τ is a root node, false otherwise
<code>$\{Q, \Omega\} \leftarrow \text{QR}(S)$</code>	$S = Q\Omega$ where Q is orthogonal, Ω is upper triangular
<code>level(τ)</code>	level of node τ , starting from 0 at the root
<code>$\{Y, J\} \leftarrow \text{ID}(S, \varepsilon_r, \varepsilon_a)$</code>	interpolative decomposition: $S \approx S(:, J)Y$

Table 1: List of helper functions for [Algorithm 1](#).

2.3. Background on Johnson–Lindenstrauss Sketching. We begin this section by stating the classical Johnson–Lindenstrauss lemma [17]. The particular version below is from [10].

LEMMA 2.2 (Johnson–Lindenstrauss (JL) Lemma [17]). *Given $\varepsilon \in (0, 1)$ and an integer m , let d be a positive integer such that $d \geq 4(\varepsilon^2/2 - \varepsilon^3/3)^{-1} \log m$. For any set P of m points in \mathbb{R}^n there exists $f : \mathbb{R}^n \rightarrow \mathbb{R}^d$ such that for all $u, v \in P$*

$$(2.4) \quad (1 - \varepsilon)\|u - v\|^2 \leq \|f(u) - f(v)\|^2 \leq (1 + \varepsilon)\|u - v\|^2.$$

[Lemma 2.2](#) does not say anything about *how* to construct f and what form it might take. In practice, f is usually chosen to be a linear map in the form of a matrix which is drawn randomly from an appropriate distribution. The following definition captures this idea.

DEFINITION 2.3 (JL Sketching Operator). *Suppose \mathcal{D} is a distribution over matrices of size $d \times n$. We say that a matrix $R \sim \mathcal{D}$ is a $(n, d, \delta, \varepsilon)$ -JL sketching operator if for any vector $x \in \mathbb{R}^n$ it satisfies*

$$\Pr_{R \sim \mathcal{D}} [|\|Rx\|^2 - \|x\|^2| > \varepsilon\|x\|^2] < \delta.$$

The condition in [Definition 2.3](#) considers length preservation of a single vector. A standard union bound argument can be used to show that a JL matrix with probability $1 - \delta$ satisfies (2.4) for all $u, v \in P$ where P contains m points, provided that d is chosen to be sufficiently large; see Remark 2.2 of [3] for a discussion about this.

Remark 2.4. For low rank matrices A with dimension $m \times n$, a highly accurate approximation can be computed with $d \ll n$ allowing us to compute our sketch $S = AR^T$ using only matrix-vector products by iterating over the d columns of R^T .

In the following subsections, we introduce three popular JL sketching operator distributions. All three satisfy the condition in [Definition 2.3](#) provided that d is large enough. Details on theoretical guarantees for each distribution appear in [sections 3](#) and [5](#).

2.3.1. Gaussian Sketching Operator. A *Gaussian sketching operator* R of size $d \times n$ has entries which are drawn independently from a normal distribution with mean zero and variance $1/d$. We indicate that R is drawn from such a distribution by writing $R \sim \text{Gaussian}(n, d)$. Gaussian sketching operators are JL sketching operators if the dimension d is sufficiently large [10]. Key advantages of Gaussian sketching operators are ease of construction and that they lend themselves to simple and clean

theoretical analysis [23, Remark 8.2]. The main downside of the Gaussian sketching operator is that it is relatively slow to apply since it has no particular structure and is dense. The sketching operators in the two subsections below address this issue by using fast structured or sparse operators, respectively.

2.3.2. Subsampled Randomized Hadamard Transform (SRHT). A *subsampled randomized Hadamard transform* (SRHT) of size $d \times n$ takes the form $R = PHD$. The matrix $D \in \mathbb{R}^{n \times n}$ is diagonal with the diagonal entries drawn independently from the Rademacher distribution, i.e., each entry is $+1$ with probability $1/2$ and -1 with probability $1/2$. The matrix $H \in \mathbb{R}^{n \times n}$ is the normalized Hadamard matrix, a deterministic unitary matrix which can be applied to a vector in $O(n \log(n))$ time instead of $O(n^2)$. The normalized Hadamard matrix can be defined recursively via $H_0 = [1]$ and $H_{2n} = [H_n, H_n; H_n, -H_n]$. Finally, $P \in \mathbb{R}^{d \times n}$ is a sparse random sampling matrix whose rows are chosen independently and uniformly at random from the set $\{\sqrt{n/d} \cdot e_j^T\}_{j=1}^n$ where $e_j \in \mathbb{R}^n$ is the j th canonical basis vector. We indicate that R is drawn in this fashion by writing $R \sim \text{SRHT}(n, d)$. An early version of the SRHT appeared in [1] where each entry of P was independently chosen to be either zero or nonzero, with the nonzero entries drawn from an appropriately scaled normal distribution.

2.3.3. Sparse Johnson–Lindenstrauss Transform (SJLT). The *sparse Johnson–Lindenstrauss transform* (SJLT) was first introduced in [19] with subsequent further analysis in [24, 9]. An SJLT matrix R of size $d \times n$ has a fixed number $\alpha \in [d]$ of nonzero entries per column. The nonzero entries are drawn independently from a scaled Rademacher distribution, taking values in $\{1/\sqrt{\alpha}, -1/\sqrt{\alpha}\}$ uniformly at random. The paper [19] proposes two different methods for randomly drawing the position of the nonzero entries in R . The first method draws the α nonzero positions for each column of R uniformly at random from $[d]$. The second method divides the length- d columns of R into d/α chunks, and for each chunk a single entry is selected uniformly at random to be nonzero. This method requires d/α to be an integer. For both methods, sampling is done for each column independently of the nonzero positions in the other columns. The two approaches to constructing an SJLT are referred to as the *graph construction* and *block construction*, respectively. Throughout the paper, we will denote an SJLT drawn using either construction by $R \sim \text{SJLT}(n, d, \alpha)$. We implement both approaches in our software and allow the user to select which one to use. We test our implementation with the block construction since it is easier to construct and performs better experimentally than the graph construction.

3. Range-finder Bounds. In this section we prove bounds for sketching operators drawn from a JL distribution to approximate the range of $A \in \mathbb{C}^{m \times n}$. That is, we aim to show that the JL sketching has the same nice property as Gaussian sketching — it contains accurate range information, resembling Theorem 10.8 in [16].

We will prove bounds of the form $\|A - QQ^*A\|^2 = \|(I - P_S)A\|^2 \leq c_n \sigma_{r+1}$ for some constant c_n dependent on n and $0 < r \leq d$. Where $S = AR^T = Q\Omega$ and $P_S = SS^\dagger$, we refer to these bounds as *range-finder bounds*. In [16] a range-finder bound is proved for Gaussian sketching operators and SRHT. We extend their results to sketching operators drawn from a distributional JL family and SJLT. We leverage many of the same tools as [16] to prove our results and restate the range-finder bounds for Gaussian sketching operators and SRHT. Our new results in this section are [Theorem 3.6](#) and [Theorem 3.11](#).

The extension of range-finder theory is necessary for [Algorithm 1](#) where an interpolative decomposition is computed for the sketch S of a low rank block which represents the range of the original low rank block. Additionally, the stopping criteria in [Algorithm 1](#) which determines when S is accurate enough to approximate the low rank block is based on the assumption that a matrix Q which is constructed from a rank revealing QR factorization of the sketch encodes the same range as A .

We begin by recalling Theorem 9.1 from [\[16\]](#) which we leverage in our proof of a range-finder bound for sketching operators that satisfy a distributional JL property defined in [Definition 2.3](#) and SJLT defined in [subsection 2.3.3](#).

Let $A \in \mathbb{C}^{m \times n}$ be a matrix with SVD $A = U\Sigma V^*$, where $U \in \mathbb{C}^{m \times n}$ and $V \in \mathbb{C}^{n \times n}$ are orthogonal matrices and $\Sigma \in \mathbb{R}^{n \times n}$ is a diagonal matrix of singular values. Let $R \in \mathbb{R}^{(r+p) \times n}$ with $d = r + p$ where r is our target rank and p is our oversampling parameter, usually set to around 10, and consider the following decomposition:

$$(3.1) \quad A = U \begin{bmatrix} \Sigma_1 & \\ & \Sigma_2 \end{bmatrix} \begin{bmatrix} V_1^* \\ V_2^* \end{bmatrix}.$$

Where $\Sigma_1 \in \mathbb{C}^{r \times r}$ and $\Sigma_2 \in \mathbb{C}^{(n-r) \times (n-r)}$ are diagonal matrices. Let

$$(3.2) \quad R_1 := V_1^* R^T \in \mathbb{C}^{r \times d}, R_2 := V_2^* R^T \in \mathbb{C}^{(n-r) \times d}.$$

The error bound for the range-finder algorithm is dependent on properties of R_1 and R_2 . We state the following theorem from [\[16\]](#) which we leverage to prove a general result about the range-finder algorithm when using matrices that satisfy the distributional JL property.

THEOREM 3.1 (Theorem 9.1 from [\[16\]](#), deterministic bound). *Let $A \in \mathbb{C}^{m \times n}$ have SVD $A = U\Sigma V^*$, and fix $r \geq 0$ and oversampling parameter $p \geq 0$. Choose a test matrix $R^T \in \mathbb{R}^{n \times d}$ and construct $Y = AR^T$. Partition Σ as in [\(3.1\)](#), and define R_1, R_2 as in [\(3.2\)](#). Assuming that R_1 has full row rank, the approximation error satisfies*

$$(3.3) \quad \|(I - P_Y)A\|^2 \leq \|\Sigma_2\|^2 + \|\Sigma_2 R_2 R_1^\dagger\|^2.$$

To prove a range-finder bound for distributional JL sketching operators, [Theorem 3.6](#), the following two lemmas will be needed. [Lemma 3.2](#) provides an upper bound for the 2-norm of any JL sketching operator.

LEMMA 3.2 (2-norm of sketch matrix). *Let $R \in \mathbb{R}^{d \times n}$ be a distributional JL sketching operator drawn from a $(n, d, \frac{\delta}{n}, \varepsilon)$ -JL distribution such that $\varepsilon, \delta \in (0, 1)$ and $d < n$. Then, with probability $1 - \delta$, we have $\|R\| \leq \sqrt{n(1 + \varepsilon)}$.*

Proof. Let $e_1, \dots, e_n \in \mathbb{R}^n$ denote the canonical basis vectors. Note that

$$(3.4) \quad \|R\| = \max_{\substack{y \in \mathbb{R}^n \\ \|y\|=1}} \|Ry\| = \max_{\substack{\beta \in \mathbb{R}^n \\ \|\beta\|=1}} \left\| R \sum_{i=1}^n \beta_i e_i \right\| \leq \max_{\substack{\beta \in \mathbb{R}^n \\ \|\beta\|=1}} \sum_{i=1}^n |\beta_i| \|Re_i\|.$$

Since $\Pr[\|Re_i\| \leq \sqrt{1 + \varepsilon}] \geq \delta/n$, a union bound therefore gives that the following holds with probability at least $1 - \delta$:

$$(3.5) \quad \|R\| \leq \max_{\substack{\beta \in \mathbb{R}^n \\ \|\beta\|=1}} \sum_{i=1}^n |\beta_i| \|Re_i\| \leq \max_{\substack{\beta \in \mathbb{R}^n \\ \|\beta\|=1}} \sum_{i=1}^n |\beta_i| \sqrt{1 + \varepsilon} \leq \sqrt{n(1 + \varepsilon)},$$

where the last equality follows from the Cauchy–Schwarz inequality. \square

Lemma 3.3 is a standard result which can be proven in the same way as Theorem 2.3 in [30] which considers the Gaussian sketching operator case. The key fact from the lemma is the lower bound on the smallest singular value of a JL sketching operator times a tall-and-skinny matrix V . This bound is required when applying **Theorem 3.1**.

LEMMA 3.3 (JL implies subspace embedding, Theorem 2.3 from [30]). *Let $R \in \mathbb{R}^{d \times n}$ be a distributional JL sketching operator drawn from a $(n, d, \frac{\delta}{5^{2r}}, \frac{\varepsilon}{12})$ -JL distribution with $\frac{\varepsilon}{12}, \delta \in (0, 1)$. Let $V \in \mathbb{C}^{n \times r}$ where $r < d < n$ be a full rank matrix. Then with probability at least $1 - \delta$ the following holds:*

$$(3.6) \quad \left| \|RVx\|^2 - \|Vx\|^2 \right| < \varepsilon \|Vx\|^2 \quad \text{for all } x \in \mathbb{R}^r.$$

Proof. See **Appendix A.1** for the details of the proof. \square

Remark 3.4. The smallest singular value of any matrix B satisfies (see, e.g., Theorem 8.6.1 in [12])

$$(3.7) \quad \sigma_{\min}^2(B) = \min_{\|x\|=1} \|Bx\|^2.$$

The statement in (3.6) therefore implies

$$(3.8) \quad \sigma_{\min}^2(RV) \geq (1 - \varepsilon)\sigma_{\min}^2(V),$$

and consequently that RV is of full rank since $\sigma_{\min}^2(V) > 0$ and $(1 - \varepsilon) > 0$.

Remark 3.5. The exponential dependence on r in the $(n, d, \frac{\delta}{5^{2r}}, \frac{\varepsilon}{12})$ in **Lemma 3.3** may seem alarming. However, for many JL sketching operator distributions the embedding dimension has a logarithmic dependence on $1/\delta$, which translates to a linear dependence on r . This is true for the Gaussian sketching operators, as well as for the SRHT and SJLT we consider in this paper.

Now that we have bounded the two norm of our JL sketching operator and proved that R_1 from (3.2) will be full rank with high probability we are ready to apply **Theorem 3.1** and prove our distributional JL range-finder bound.

THEOREM 3.6 (Distributional JL implies Range-finder Bound). *Suppose $A \in \mathbb{C}^{m \times n}$ is a matrix and let $0 < r < \min(m, n)$ be the target rank. If R is a $(n, d, \frac{\delta}{2 \max(5^{2r}, n)}, \frac{\varepsilon}{12})$ -JL sketching operator with $\varepsilon/12, \delta \in (0, 1)$ and $d = r + p$ with $p \geq 0$, then the following holds with probability at least $1 - \delta$:*

$$(3.9) \quad \|(I - P_Y)A\| \leq \left(\sqrt{1 + \frac{n(1 + \varepsilon)}{(1 - \varepsilon)}} \right) \sigma_{r+1}(A),$$

where $Y = AR^T$.

Proof. From **Lemma 3.2**, **Lemma 3.3** and **Remark 3.4** we have that the following two events happen simultaneously with probability at least $1 - \delta$:

$$(3.10) \quad \|R\| \leq \sqrt{n(1 + \varepsilon)} \quad \text{and} \quad \sigma_{\min}^2(RV) \geq (1 - \varepsilon)\sigma_{\min}^2(V).$$

We proceed under the assumption that the events in (3.10) occur.

Due to (3.10), R_1 is full rank, and **Theorem 3.1** therefore yields

$$(3.11) \quad \|(I - P_Y)A\|^2 \leq \|\Sigma_2\|^2 + \|\Sigma_2 R_2 R_1^\dagger\|^2.$$

Taking the square root of both sides and using the sub-multiplicativity of the two norm we have

$$(3.12) \quad \|(I - P_Y)A\| \leq \sqrt{\|\Sigma_2\|^2 + \|\Sigma_2\|^2\|R_2\|^2\|R_1^\dagger\|^2} = \sqrt{\|\Sigma_2\|^2(1 + \|R_2\|^2\|R_1^\dagger\|^2)}.$$

To bound $\|R_2\|^2$, note that

$$(3.13) \quad \|R_2\|^2 = \|V_2^* R^T\|^2 = \|R^T\|^2 \leq n(1 + \varepsilon),$$

where the second equality follows from unitary invariance of the two norm, and inequality follows from (3.10). To bound $\|R_1^\dagger\|^2$, note that

$$(3.14) \quad \|R_1^\dagger\|^2 = \frac{1}{\sigma_{\min}^2(R_1)} \leq \frac{1}{(1 - \varepsilon)\sigma_{\min}^2(V_1)} = \frac{1}{1 - \varepsilon}$$

where the inequality follows from (3.10). Combining (3.12), (3.13) and (3.14) and the fact that $\|\Sigma_2\| = \sigma_{r+1}(A)$ results in the bound (3.9). \square

Next we restate the range-finder bounds for Gaussian sketching operators and SRHT from [16].

THEOREM 3.7 (Corollary 10.9 from [16], simplified deviation bounds of Theorem 10.8). *Suppose that $A \in \mathbb{C}^{m \times n}$ has singular values $\sigma_1 \geq \sigma_2 \geq \sigma_3 \geq \dots$. Choose oversampling parameter $p \geq 4$ and target rank $r \geq 2$, where $r + p \leq \min(m, n)$. Draw an $R^T \in \mathbb{R}^{n \times (r+p)}$ with standard Gaussian entries and construct the sketch matrix $Y = AR^T$. Then the norm squared approximation error is*

$$\|(I - P_Y)A\| \leq \left(1 + 16\sqrt{1 + \frac{r}{p+1}}\right)\sigma_{r+1}(A) + \frac{8\sqrt{r+p}}{p+1} \left(\sum_{j>r} \sigma_j^2(A)\right)^{1/2},$$

with probability at least $1 - 3e^{-p}$.

Remark 3.8. The above theorem states that R has standard Gaussian entries but we consider a Gaussian sketching operator where the variance of the Gaussian entries is $1/d$ corresponding to scaling all of the standard Gaussian entries by $1/d$. Since we use the sketch $Y = AR^T$ to construct a projection operator this scaling cancels out and the projection operator remains the same for both the scaled and unscaled Gaussian sketching operators thus the above result also holds for Gaussian sketching operators.

THEOREM 3.9 (Theorem 11.2 from [16]). *Suppose that $A \in \mathbb{C}^{m \times n}$ has singular values $\sigma_1(A) \geq \sigma_2(A) \geq \sigma_3(A) \geq \dots$. Choose oversampling parameter $p \geq 1$ and target rank $r \geq 1$ such that $r + p \leq \min\{m, n\}$ and*

$$4 \left[\sqrt{r} + \sqrt{8 \log(rn)} \right]^2 \leq (r + p) \leq n.$$

Draw an $R \in \mathbb{R}^{(r+p) \times n}$ SRHT and construct the sketch matrix $Y = AR^T$. Then the norm squared approximation error is

$$\|(I - P_Y)A\| \leq \sqrt{1 + 7n/(r+p)} \cdot \sigma_{r+1}(A),$$

with failure probability at most $O(r^{-1})$.

Remark 3.10. The above result in [16] is stated when the fast transform is a discrete Fourier transform but in this paper we apply the Hadamard transform. The identical result holds for the Hadamard transform by combining the result in [27] and following the identical steps of the proof for with Fourier transform in [16].

Finally, we state a range-finder bound for SJLT. The proof of [Theorem 3.11](#) can be found in [Appendix A.2](#) which follows the steps of the proof of [Theorem 3.6](#) but with stronger guarantees since it is restricted to SJLT matrices.

THEOREM 3.11. *Given matrix $A \in \mathbb{C}^{m \times n}$ and a rank $r < \min(m, n)$. Fix $\varepsilon, \delta \in (0, 1)$. If $R \sim \text{SJLT}(n, d, \alpha)$ with $\alpha = \Theta(\log^3(r/\delta)/\varepsilon)$, $d = \Omega(r \log^\delta(r/\delta)/\varepsilon^2)$ and $Y = AR^T$ then*

$$(3.15) \quad \|(I - P_Y)A\| \leq \sigma_{r+1}(A) \sqrt{1 + \frac{1}{(1-\varepsilon)} \max\left(\frac{\varepsilon^2 n \alpha}{d}, \log\left(\frac{2d}{\delta}\right) - \frac{n\alpha}{d}\right)}.$$

with probability $1 - \delta$.

In summary, the new foundational theory in this section is [Theorem 3.6](#), which shows that a projection based on a distributional JL sketching operator achieves good approximation of the range of the original matrix. With similar proof techniques, we show that the SJLT sketching achieves good range approximation as well ([Theorem 3.11](#)). These two new results augment the existing range-finder bounds for the Gaussian sketching operators and SRHT matrices justifying our use of a more general class of sketching operators in our HSS compression algorithm.

4. Stopping Criteria for Adaptive HSS Algorithm. For any adaptive algorithm, it is critical to develop robust stopping criteria. For us, we would like sufficiently large sketches (enough columns of $S = AR^T$) to ensure accuracy but not too large which hurts performance.

Since we leverage $S = AR^T \in \mathbb{C}^{n \times d}$, the sketch, instead of $A \in \mathbb{C}^{n \times n}$, the true matrix, we must determine how many columns of $R^T \in \mathbb{R}^{n \times d}$ are necessary on the fly which corresponds to approximating the HSS rank r of our matrix in which $r < d \ll n$. We use a block incrementing strategy where we begin with $d = d_0 + \Delta d$, check if the last Δd columns contain new range information and add Δd columns iteratively as long as there is sufficient range information in the new columns of the sketch. This can be thought of as extending the sketching operator or applying additional sketching operators to gain new information about the range of the low dimensional Hankel blocks of A . In our HSS compression algorithm we have two types of stopping criteria: Frobenius norm criteria and rank deficiency criteria, [line 27](#) and [line 31](#) of [Algorithm 1](#) respectively.

One contribution in [13] is the development of the Frobenius norm stopping criteria. First, a stochastic Frobenius norm relationship between the matrix $\|A\|_F$ and the sketch $\|S\|_F$ was established, when the sketching operator R^T has i.i.d. standard Gaussian entries with mean zero and variance one. Additionally, it was shown that $\mathbb{E}[\|\frac{1}{\sqrt{d}}S\|_F^2] = \|A\|_F^2$, and a concentration bound was established detailing that when R^T has more columns the sketch matrix and original matrix Frobenius norms are likely closer. The significance of this theoretical result is that we can use the projection error based on the sketch to stop the iteration instead of the original matrix A (A is not available in many applications). An additional benefit is that using stopping criteria based on S allows the compression algorithm to be partially matrix-free. R^T is a skinny matrix so S can be computed exclusively via matrix-vector products.

Moreover the sketch can be used for both absolute and relative error estimates. The goal of the Frobenius norm stopping criteria is to check if adding an additional Δd columns of the sketch will significantly improve the compression.

The Frobenius norm stopping criteria are:

$$(4.1) \quad \frac{\|\widehat{S}\|_F}{\|\widetilde{S}\|_F} < \varepsilon_{\text{rel}}, \quad \|\widehat{S}\|_F < \varepsilon_{\text{abs}}.$$

Where $\widetilde{S} = A_{\nu_i, \nu_j} \bar{R}^T$ is a matrix of the Δd new sketch for our Hankel block and $\widehat{S} = (I - Q_\tau Q_\tau^*) \widetilde{S}$ is the projection of the new sketch onto the orthogonal complement of the current sketch of the Hankel block (Q_τ is constructed from $A_{\nu_i, \nu_j} R^T$). If $\|\widehat{S}\|_F$ is small either relative to the first d columns of the sketch or absolutely then extending the sketch matrix to include additional columns will likely only yield a small amount of information at a large cost of memory in the construction so the sketch matrix is not extended more and the stopping criteria are met.

Remark 4.1. We have updated the stopping condition $\frac{1}{\sqrt{d}} \|\widehat{S}\|_F < \varepsilon_{\text{abs}}$ in [13] to $\|\widehat{S}\|_F < \varepsilon_{\text{abs}}$ because now we scale the sketching operator R^T so that it satisfies the JL sketching operator definition, removing the need for $\frac{1}{\sqrt{d}}$ scaling.

Remark 4.2. In the implementation we set $\widehat{S} = (I - Q_\tau Q_\tau^*)^2 \widetilde{S}$, which applies two steps of block Gram-Schmidt for projection to ensure orthogonality under roundoff errors [25].

For these criteria to work well, we need our sketch matrix to be close to our true matrix in the Frobenius norm. Section 5 provides guarantees on how close we can expect the Frobenius norm for a matrix M , $\|M\|_F^2$, to be to $\|MR^T\|_F^2$ when R is an arbitrary JL sketching operator, as well as when it is a Gaussian sketching operator, SRHT or SJLT (see Section 2 for the construction of these sketches). We can frame the block incrementing strategy as extending the rows of the sketching operator R or drawing a new sketching operator with Δd rows. We provide a table (Table 2) summarizing our theoretical results in which we provide a lower bound on d , the number of columns of R^T , such that the following holds with probability at least $1 - \delta$:

$$(1 - \varepsilon) \|M\|_F^2 \leq \|MR^T\|_F^2 \leq (1 + \varepsilon) \|M\|_F^2.$$

Additionally, we prove Theorem 5.1 which provides the same guarantee for any JL sketching operator.

Sketching Operator	Frobenius Norm Bound
Gaussian	$d \geq 20\varepsilon^{-2} \log(2/\delta)$ (Theorem 5.2)
SRHT	$d \geq 2\varepsilon^{-2} \log^2(4n^2/\delta) \log(4/\delta)$ (Theorem 5.3)
SJLT	$d \geq C\varepsilon^{-2} \log(1/\delta)$ (Theorem 5.4)

Table 2: Convergence guarantees for Frobenius norm stopping criterion.

These bounds are known to be conservative, requiring d to be quite large. For example, if we use a Gaussian sketching operator and set our failure probability $\delta = 0.01$ and $\varepsilon = 0.5$ then we have the bound $d \geq 424$ for $(0.5) \|A\|_F^2 \leq \|AR^T\|_F^2 \leq$

(1.5) $\|A\|_F^2$ to hold with probability at least 0.99. In practice it works well to choose $d_0 = 128$ and $\Delta d = 64$ (STRUMPACK library default values).

If the Frobenius norm criteria are not satisfied we may not have a sufficiently representative sketch. We then check the rank deficiency stopping criteria which first requires that we compute and augment our current Q matrix, representing the range of our current sketch, lines 29-30 in [Algorithm 1](#). We then check the smallest diagonal entry of the upper triangular matrix from our QR factorization. This check corresponds to verifying that the columns which we augment to Q (line 30 of [Algorithm 1](#)) are representative of the range of our sketch and not just added to satisfy the orthogonality requirement for Q . If the diagonal entries are small this would mean that the extension of our sketch is close to rank deficient or that the corresponding column of Q does not encode information about our low rank block.

The rank deficiency stopping criteria are

$$(4.2) \quad \frac{\min_i |\widehat{\Omega}_{ii}|}{(\Omega_1)_{11}} < \varepsilon_{\text{rel}}, \quad \min_i |\widehat{\Omega}_{ii}| < \varepsilon_{\text{abs}}.$$

If either of these rank deficiency stopping criteria are met then the sketching is representative of the original low rank block and compression can occur. Since the interpolative decomposition is computed using a rank revealing QR factorization, the stopping criteria calculations will likely yield successful compression.

In the next section, we extend the theory necessary to justify the Frobenius norm stopping criteria. That is, the more columns added to our sketching operator R^T the closer our sketch S will be to A in terms of Frobenius norm.

5. Frobenius Norm Bounds. In this section, we present the mathematical theory to support the use of the Frobenius norm bound as one of the stopping criteria discussed in [Section 4](#). The new result in this Section is [Theorem 5.1](#), which is a unified, foundational theorem about the concentration bound for general JL sketching operators. We will then make the connection of this theorem with the existing theory in the literature, sharpening the bounds for specific types of JL sketching operators, including Gaussian sketching operators, SRHT, and SJLT. The unified framework provides theoretical lower bounds on the number of samples, columns of the sketching operator, d needed in each case to achieve the approximation guarantee in a probabilistic sense.

The first result provides a Frobenius norm concentration result which holds for any real JL sketching operator.

THEOREM 5.1. *Let $A \in \mathbb{C}^{m \times n}$ and $\varepsilon, \delta \in (0, 1)$. If $R \in \mathbb{R}^{d \times n}$ is a $(n, d, \delta', \varepsilon)$ -JL matrix where $\delta' = \delta/m$ if A is real and $\delta' = \delta/(2m)$ if A is complex, then the following holds with probability at least $1 - \delta$:*

$$(5.1) \quad (1 - \varepsilon)\|A\|_F^2 \leq \|AR^T\|_F^2 \leq (1 + \varepsilon)\|A\|_F^2.$$

Proof. Consider first the case when A is real. Since R is a $(n, d, \frac{\delta}{m}, \varepsilon)$ -JL matrix it satisfies

$$(5.2) \quad \Pr \left[\left| \|x^T R^T\|^2 - \|x^T\|^2 \right| > \varepsilon \|x^T\|^2 \right] < \frac{\delta}{m}$$

for any $x \in \mathbb{R}^n$. Let A_j denote the j th row of A . By the triangle inequality,

$$(5.3) \quad \left| \|AR^T\|_F^2 - \|A\|_F^2 \right| = \left| \sum_{j=1}^m \left(\|A_j R^T\|^2 - \|A_j\|^2 \right) \right| \leq \sum_{j=1}^m \left| \|A_j R^T\|^2 - \|A_j\|^2 \right|.$$

Consequently,

$$\begin{aligned}
(5.4) \quad \Pr \left[\left| \|AR^T\|_F^2 - \|A\|_F^2 \right| > \varepsilon \|A\|_F^2 \right] &\leq \Pr \left[\sum_{j=1}^m \left| \|A_{j:}R^T\|^2 - \|A_{j:}\|^2 \right| > \varepsilon \sum_{k=1}^m \|A_{j:}\|^2 \right] \\
&\leq \Pr \left[\bigcup_{j=1}^m \left(\left| \|A_{j:}R^T\|^2 - \|A_{j:}\|^2 \right| > \varepsilon \|A_{j:}\|^2 \right) \right] \\
&\leq \sum_{j=1}^m \Pr \left[\left| \|A_{j:}R^T\|^2 - \|A_{j:}\|^2 \right| > \varepsilon \|A_{j:}\|^2 \right] \\
&< m \frac{\delta}{m} = \delta,
\end{aligned}$$

where the third inequality is a union bound and the final inequality follows from (5.2). This proves the result for the real case.

For the complex case, we may write $A = B + \hat{i}C$ where $B, C \in \mathbb{R}^{m \times n}$. Since

$$(5.5) \quad \|A\|_F^2 = \left\| \begin{bmatrix} B \\ C \end{bmatrix} \right\|_F^2, \quad \|AR^T\|_F^2 = \left\| \begin{bmatrix} B \\ C \end{bmatrix} R^T \right\|_F^2,$$

and R is a $(n, d, \delta/(2m), \varepsilon)$ -JL matrix, the complex case follows from the result when A is real (proved above). \square

The statement in [Theorem 5.1](#) can be strengthened when specific sketching operators are considered. We state known bounds for the Gaussian sketching operators ([Theorem 5.2](#)), SRHT ([Theorem 5.3](#)) and SJLT ([Theorem 5.4](#)). The statements in [Theorems 5.2](#) and [5.3](#) follow directly from [Theorems 5.2](#) and [8.4](#) in [2]; see [Appendix A.3](#) for details.

THEOREM 5.2 (Theorem 5.2 in [2]). *Let $A \in \mathbb{C}^{m \times n}$ be a matrix and suppose $R \sim \text{Gaussian}(n, d)$. If $d \geq 20\varepsilon^{-2} \log(2/\delta)$, then the following holds with probability at least $1 - \delta$:*

$$(5.6) \quad (1 - \varepsilon) \|A\|_F^2 \leq \|AR^T\|_F^2 \leq (1 + \varepsilon) \|A\|_F^2.$$

In [13] a different concentration bound is stated for the Gaussian case dependent on the singular values of A .

THEOREM 5.3 (Theorem 8.4 in [2]). *Let $A \in \mathbb{C}^{m \times n}$ be a matrix and suppose $R \sim \text{SRHT}(n, d)$. If $d \geq 2\varepsilon^{-2} \log^2(4n^2/\delta) \log(4/\delta)$, then the following holds with probability at least $1 - \delta$:*

$$(5.7) \quad (1 - \varepsilon) \|A\|_F^2 \leq \|AR^T\|_F^2 \leq (1 + \varepsilon) \|A\|_F^2.$$

The result in [Theorem 5.4](#) below is a matrix variant of the main result in [19]. It can be proven with a slight modification to a proof in [9] which provides a simplified analysis of the result in [19]. For completeness, we provide this modified proof in [Appendix A.4](#).

THEOREM 5.4 (Matrix version of result in [19]). *Let $A \in \mathbb{C}^{m \times n}$ be a matrix and suppose $R \in \mathbb{R}^{d \times n}$ is an SJLT constructed using either the graph or block construction (see [subsection 2.3.3](#)), and suppose $\varepsilon \in (0, 1)$ and $\delta \in (0, 1/2)$. If $d \geq C\varepsilon^{-2} \log(1/\delta)$*

and $\alpha = \lceil \varepsilon d \rceil$ where C is an absolute constant, then the following holds with probability at least $1 - \delta$:

$$(5.8) \quad (1 - \varepsilon)\|A\|_F^2 \leq \|AR^T\|_F^2 \leq (1 + \varepsilon)\|A\|_F^2.$$

These bounds are conservative – in practice, we find that fewer samples are sufficient for good compression. From a theoretical standpoint, Gaussian sketching operators require fewer samples than SRHT and SJLT. Although, SJLT and SRHT can be applied faster leading to a trade off between speed and accuracy. In the following sections we will examine efficiently implementing an SJLT sketching routine and compare it to the existing Gaussian sketching routine. We will observe that we can achieve faster compression time with similar accuracy when applying SJLT sketching over Gaussian sketching.

6. SJLT Sketching Implementation Details. The SJLT matrix is a highly structured random matrix. To leverage this structure we have created an SJLT data structure and custom sketching routines that use the SJLT data structure. Our specialized data structure and sketching routines speed up the HSS compression algorithm by leveraging matrix sparsity and bypassing multiplications.

6.1. SJLT Data Structure. An SJLT matrix is a structured sparse matrix whose entries have two possible nonzero values. $R^T \in \mathbb{R}^{n \times d}$ is an SJLT matrix with α nonzeros in each row with each nonzero drawn from $\{1/\sqrt{\alpha}, -1/\sqrt{\alpha}\}$ with equal probability. We factor out and store the scaling of $1/\sqrt{\alpha}$ and split our matrix into positive and negative components, resulting in $R^T = 1/\sqrt{\alpha}(B_+ - B_-)$, where the matrices B_+ and B_- only have entries in $\{0, 1\}$. Since B_+ and B_- are sparse binary matrices we store them in compressed form. We use both compressed row storage (CRS) and compressed column storage (CCS) [4] where we store pointers to the start of each row (CRS) or column (CCS), and the column or row indices of the nonzero entries respectively. Since our matrices are binary the nonzero values are always one so we do not need to store the values at these nonzero positions. We store the binary matrices in both compressed row and column storage to leverage the caching of the dense matrix A when computing AR^T and A^*R^T . Below we provide an example of our data structure and decomposition.

$$R^T = \frac{1}{\sqrt{2}} \begin{bmatrix} 1 & 0 & -1 \\ 0 & -1 & -1 \\ 1 & -1 & 0 \\ 1 & 0 & 1 \end{bmatrix} = \frac{1}{\sqrt{2}} \left(\begin{bmatrix} 1 & 0 & 0 \\ 0 & 0 & 0 \\ 1 & 0 & 0 \\ 1 & 0 & 1 \end{bmatrix} - \begin{bmatrix} 0 & 0 & 1 \\ 0 & 1 & 1 \\ 0 & 1 & 0 \\ 0 & 0 & 0 \end{bmatrix} \right) = \frac{1}{\sqrt{2}}(B_+ - B_-)$$

$$R^T : \begin{cases} s = \frac{1}{\sqrt{2}} \\ B_+ \text{ stored in CRS and CCS without value arrays} \\ B_- \text{ stored in CRS and CCS without value arrays} \end{cases}$$

This specialized SJLT data structure for binary matrices allows us to avoid doing any multiplications in our algorithm because all multiplications would be by the number one. Instead, we only need to index and sum relevant values. Then after our matrix multiplication is complete we can scale all entries in our resulting sketch. Additionally, storing the SJLT as a sum of two binary compressed matrices requires

less space than as a single compressed matrix which additionally includes the value at each nonzero position when the number of nonzero entries per row is strictly greater than one. Finally, the SJLT data structure is well integrated in the HSS compression algorithm. Since we adaptively append additional SJLT matrices to the end of our existing SJLT matrix for improved accuracy we can efficiently update our SJLT data structure by changing the scaling factor and appending additional binary columns to the existing SJLT matrix.

6.2. Computing AR^T . In the C++ STRUMPACK library a dense matrix A is stored in column major ordering, so to leverage caching we would like to access our large dense matrix A column by column. We implement the sketching of A , AR^T by considering the outer product formulation.

$$AR^T = \begin{bmatrix} | & | & & | \\ A_{:1} & A_{:2} & \dots & A_{:n} \\ | & | & & | \end{bmatrix} \begin{bmatrix} - & R_{1:} & - \\ - & R_{2:} & - \\ & \vdots & \\ - & R_{n:} & - \end{bmatrix} = \sum_{i=1}^n A_{:i}R_{i:}.$$

First we initialize a zero matrix which will store our solution and factor out the scaling factor s from our matrix R^T . We iterate over each row of R^T in compressed row storage. For each row R_i^T if entry ij is 1, corresponding to a nonzero entry in B_+ , then we add column A_i to column j of our solution matrix. If entry ij is -1 , corresponding to a nonzero entry in B_- , then we subtract column A_i from column j of our solution matrix. This algorithm allows us to access each column of A once and based on the row R_i^T add or subtract it to different positions in our solution matrix. Since our solution matrix is much smaller than the matrix A this trade-off of leveraging caching of A while accessing many entries in our solution matrix is advantageous. Finally, we scale the resulting matrix after we have completed our sketching routine.

6.3. Computing A^*R^T . In the HSS compression algorithm we compute the sketch for both the rows and the columns of our input dense matrix A . This means that in our STRUMPACK implementation in addition to computing AR^T we must also compute A^*R^T . Since we only store A and it is stored in column major format we leverage an inner product formulation for this sketching routine. Where

$$A^*R^T = \begin{bmatrix} | & | & & | \\ A_{:1} & A_{:2} & \dots & A_{:n} \\ | & | & & | \end{bmatrix}^* \begin{bmatrix} | & | & & | \\ R_{:1} & R_{:2} & \dots & R_{:k} \\ | & | & & | \end{bmatrix}.$$

So to compute this sketch we iterate over each column of A which allows us to leverage caching. Then we take an inner product between the complex conjugate of this column of A and each column of R^T which we do by using compressed column storage, ignoring the scaling factor. This corresponds to entries in our resulting matrix. Each entry in the resulting matrix is a scaled sum of either $+1$, -1 or 0 times each entry of the column of A so no multiplication is necessary in this computation. Finally, we can scale the entire result matrix afterwards.

7. Experimental Results. In this section we compare our HSS construction algorithm using Gaussian sketching operators and SJLT matrices with different numbers of nonzero entries per row. We observe that the accuracy of the construction is

comparable between both types of sketching operators when $\alpha > 1$ while the SJLT sketching can be done faster.

We consider the following test cases:

1. A covariance matrix, using an exponential kernel

$$(7.1) \quad G_{ij} = \exp\left(-\frac{\|x_i - x_j\|_2}{\lambda}\right)$$

with $x_i, x_j \in [0, 1]^3$ and $\lambda = .2$ the correlation length. We use a structured hexahedral finite element mesh, discretized using the MFEM finite element library. The matrix is reordered using recursive bisection, which also defines the HSS cluster tree.

2. A Toeplitz matrix describing a 1D kinetic energy quantum chemistry problem [18], given by

$$(7.2) \quad T_{ij} = \begin{cases} \pi^2 / (6d^2) & \text{if } i = j \\ (-1)^{i-j} / (d^2 (i-j)^2) & \text{else} \end{cases}$$

where $d = 0.1$ is a discretization parameter (grid spacing). The matrix T is fairly ill-conditioned and has small HSS ranks which grow slowly with the dimension of T .

3. The impedance matrix Z [21]:

$$(7.3) \quad Z_{ij} = \frac{k\eta_0}{4} \int_S t_i(\rho) \int_S b_j(\rho') H_0^{(2)}(k|\rho - \rho'|) ds' ds$$

where $k = 2\pi/\lambda_0$ is the wave number, λ_0 denotes the free-space wavelength, η_0 is the intrinsic impedance of free space, and $H_0^{(2)}$ is the zeroth-order Hankel function of the second kind. The surface S is a perfectly electrically conducting circle (2D) residing in free space. This circle is discretized using n line segments, and we use delta functions located at the center of each line segment for t_i , and constant functions supported on the line segments for b_j . The inner integral is evaluated with a simple quadrature rule with 4 quadrature points. For the experiments we vary n and adjust λ_0 accordingly such that the number of points per wavelength is approximately 24.

4. The root front from a sparse multifrontal solver [11]. The multifrontal solver is applied to a linear system resulting from the second order central finite difference discretization of the 3D Poisson equation on a k^3 grid, with zero Dirichlet boundary conditions. The sparse solver uses a nested dissection ordering, and the root vertex separator, a $k \times k$ plane in the grid, corresponds to the dense $k^2 \times k^2$ root frontal matrix.

The HSS construction algorithm with the different sketching options, and the test cases are implemented in the STRUMPACK library, and are available at <https://github.com/pghysels/STRUMPACK/>. All experiments are run on a desktop with an AMD Ryzen 9 3950X and 128GB of DDR4 memory. The code is compiled with GCC 12.2, and the BLAS/LAPACK routines are from OpenBLAS 0.3.20. We run with 8 OpenMP threads. The adaptive HSS construction uses $d_0 = 128$ and $\Delta d = 64$. The HSS leaf size is set to 256. In the experiments, we vary the relative HSS compression tolerance ε_{rel} , and keep the absolute compression tolerance at $\varepsilon_{\text{abs}} = 10^{-8}$. Random numbers are generated using the C++11 `std::minstd_rand` linear congruential engine.

Matrix	ε_{rel}	n	HSS sketching time (ms)					Total HSS construction time (ms)					comp (%)
			G	S(1)	S(2)	S(4)	S(8)	G	S(1)	S(2)	S(4)	S(8)	
Cov.	10^{-2}	10^3	3	1	1	2	4	16	10	11	13	15	46.1
		20^3	393	146	166	224	366	612	312	333	392	548	7.5
		30^3	6632	2194	2470	3506	5456	7687	3053	3425	4400	6324	2.2
	10^{-4}	10^3	3	1	1	3	6	31	14	31	26	29	58.0
		20^3	1282	581	669	843	1459	2835	2082	2212	2363	2893	19.3
		30^3	36416	13466	15943	21668	33530	64070	41899	44416	49208	61487	11.2
	10^{-6}	10^3	7	1	2	5	9	51	21	54	61	57	73.9
		20^3	1844	777	911	1259	2189	5479	4104	4275	4842	5677	30.5
		30^3	48224	18032	21280	28923	46099	115034	85233	90575	96433	110408	18.1
QChem Toeplitz	10^{-2}	10K	288	72	85	112	187	347	94	115	136	213	1.7
		20K	1171	295	316	402	682	1287	345	363	446	749	0.9
		40K	4552	1366	1645	2273	3441	4792	1498	1775	2392	3577	0.4
	10^{-4}	10K	287	74	84	113	183	342	108	117	140	220	1.9
		20K	1160	294	313	404	679	1276	342	364	455	739	0.9
		40K	4576	1370	1672	2264	3409	4803	1514	1813	2411	3580	0.5
	10^{-6}	10K	289	72	84	112	189	350	101	119	144	232	2.0
		20K	1165	295	317	407	677	1294	356	389	467	745	1.0
		40K	4569	1368	1658	2243	3456	4816	1519	1822	2413	3631	0.5
Scatt. wave	10^{-2}	5K	276	69	76	100	154	392	167	166	201	252	4.7
		10K	1754	493	544	655	1005	2226	911	965	1106	1446	2.7
		20K	12360	4184	4344	5324	7703	14855	6446	6533	7481	10008	1.6
	10^{-4}	5K	276	71	78	102	155	393	175	175	203	255	5.1
		10K	1761	508	545	659	1018	2251	955	982	1099	1491	2.9
		20K	13668	4580	4675	5659	8413	16612	7329	7424	8477	11306	1.8
	10^{-6}	5K	276	71	79	102	156	417	186	203	218	273	5.4
		10K	1760	501	551	669	1013	2294	965	1030	1147	1515	3.1
		20K	12210	4600	4669	5630	8432	14762	7382	7469	8449	11370	1.9
3D Poisson front	10^{-2}	75^2	248	252	172	161	265	471	853	484	355	467	14.2
		100^2	1061	1307	515	663	1073	1774	5081	1221	1289	1720	11.2
		125^2	3431	3557	1458	1963	3175	5207	10198	3106	3606	4865	9.2
	10^{-4}	75^2	350	181	176	253	401	826	767	582	698	820	22.5
		100^2	1561	635	783	1089	1752	3004	2348	2402	2548	3286	17.9
		125^2	4874	1907	2300	3214	5116	8556	5377	6068	6671	8764	15.0
	10^{-6}	75^2	501	210	263	340	589	1199	885	958	1023	1250	27.7
		100^2	2382	952	1160	1644	2582	5251	4001	4018	4528	5536	23.0
		125^2	7315	2871	3412	4690	7389	14282	10053	10891	11720	14382	18.7

Table 3: Timing results for HSS compression, and sketching time. G refers to sketching with a Gaussian sketching operator, $S(\alpha)$ to sketching with an SJLT matrix (block construction) with α nonzeros per row.

Table 3 shows timing results for these 4 test cases, for different dimensions and compression tolerances. In this table, the HSS construction time includes the sketching time. The final column shows the memory usage for the HSS matrix as a percentage of the storage requirements for the corresponding dense matrix. This means that if $n\%$ is listed in the table, $n\%$ of the space required to store a dense matrix A is required to store an HSS compressed version.

The timings for the largest matrices of each test case are also shown in Figure 2 where blue represents the sketching step for each run and red represents the remaining HSS construction time. Additionally, we list the ratio of total time to run the compression algorithm in relation to the Gaussian case. Frequently, we observe that with $\text{SJLT}(\alpha = 1)$ we achieve a 2 – 3 times speedup and when we use $\alpha = 2$ or 4 we achieve a 1.5 – 2.5 times speedup. We observed that the random matrix construction time is negligible in both the Gaussian and SJLT cases. For the 3D Poisson frontal matrix with 125^2 rows, $\text{SJLT}(\alpha = 1)$ is significant slower than Gaussian sketching for $\varepsilon_{\text{rel}} = 10^{-2}$. As can be seen from Figure 7, this is caused by severe overestimation of the HSS rank, meaning that many more adaptive steps must be taken and much

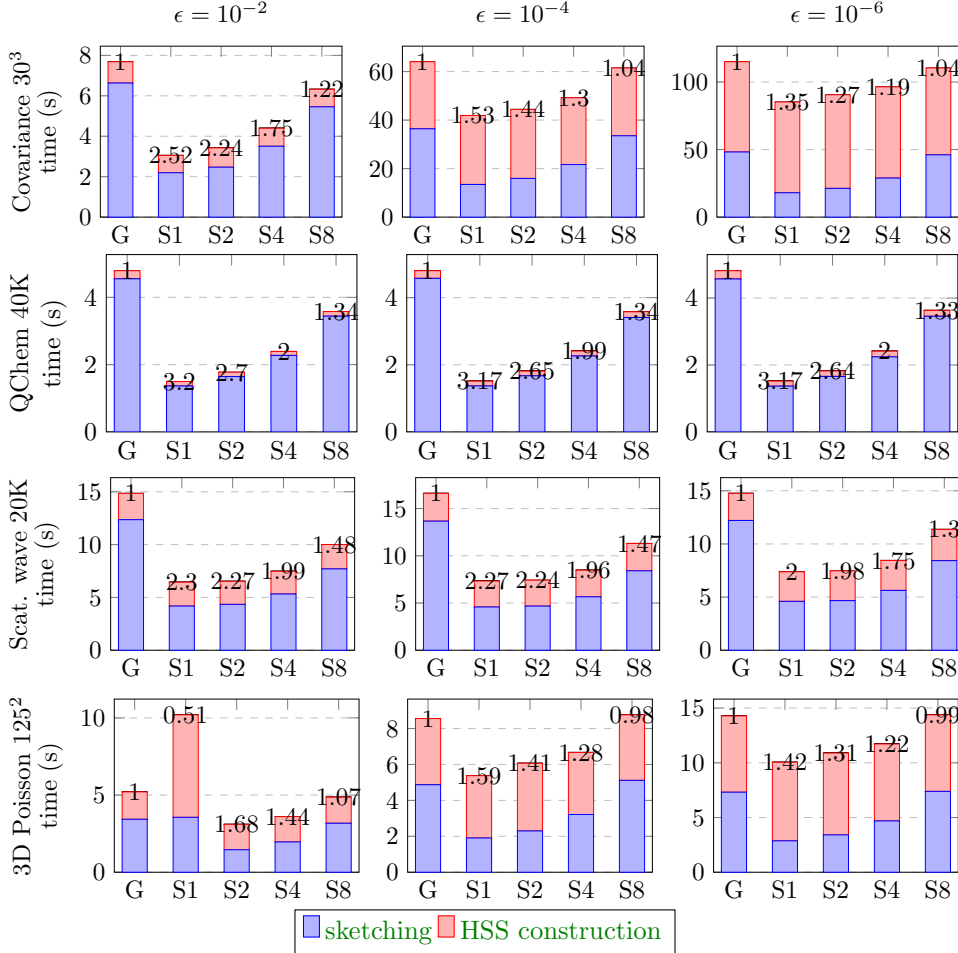


Fig. 2: HSS construction time and sketching time. Overall speedup compared to Gaussian sketching is shown at the top of each bar.

larger off diagonal low rank approximations are computed.

Figure 3 shows the oversampling ratio, i.e., the ratio of the final d (without Δd) over the HSS rank r , for the largest test problems. The quantum chemistry Toeplitz problem is omitted, since the ranks are so small that no adaptation is required. The oversampling ratio is similar for the different sketching methods.

Finally, Figures 4 to 7 show the relative errors and the HSS ranks for these problems. For these results, the experiments are run 5 times and the figures show error bars with the minimum, median and maximum values. We observe that the HSS ranks and errors are comparable between all of the sketching operators except for SJLT with $\alpha = 1$, in which performance in terms of rank and error are worse than Gaussian sketching operators.

We recommend that users of STRUMPACK use the default values of $d_0 = 128, \Delta d = 64$ when running the HSS compression algorithm. Additionally, if using SJLT matrices we recommend setting $\alpha = 2$ or $\alpha = 4$, the default value. We have

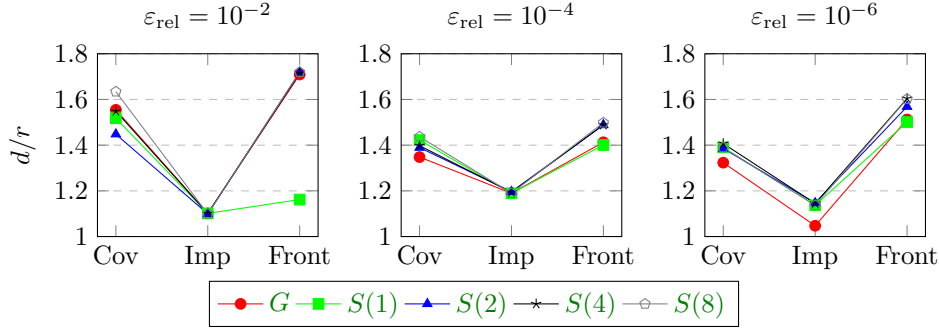


Fig. 3: Oversampling ratios, the final d (without Δd) over the HSS rank, for the largest test cases, covariance, impedance matrix (scattering wave), and frontal matrix. The quantum chemistry Toeplitz problem is omitted, since for this problem the rank are so small that it does not require any adaptation.

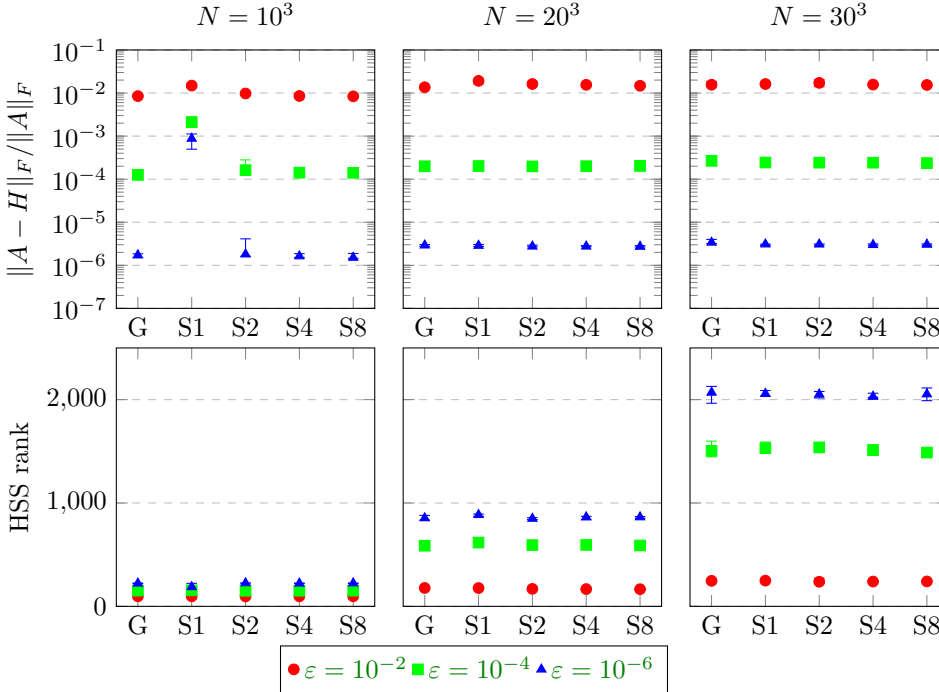


Fig. 4: Covariance matrix HSS construction relative error and maximum off-diagonal ranks.

found that this is usually the correct balance between performance improvement over Gaussian sketching operators while having similar accuracy.

8. Conclusions. In this paper we extend the adaptive HSS compression algorithm from [13] which required a Gaussian sketching operator to use any Johnson–Lindenstrauss sketching operator. We provide theoretical guarantees that the adap-

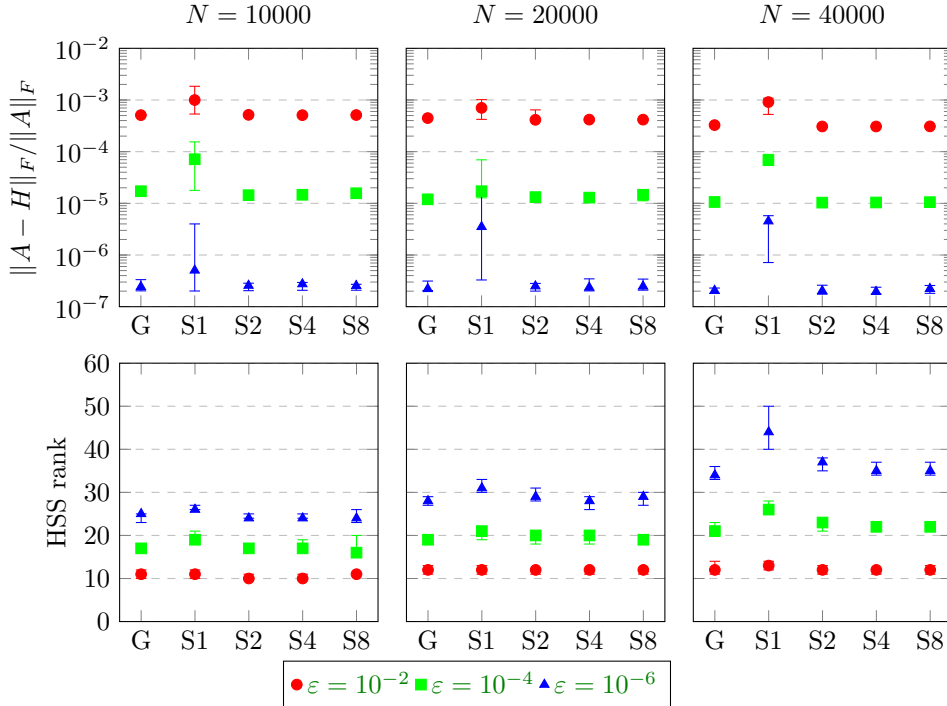


Fig. 5: Quantum Chemistry Toeplitz matrix HSS construction relative error and maximum off-diagonal ranks.

tive stopping criterion holds for all JL sketching operators including both a concentration bound in terms of Frobenius norm and a range-finder guarantee. We implement the Sparse Johnson–Lindenstrauss Transform from [19] as a use case for the more general HSS compression algorithm and examine when such a transform outperforms the Gaussian sketching operator. We provide the code in the STRUMPACK C++ library².

Acknowledgments. We acknowledge the Scalable Solvers Group in the Applied Math and Computational Research Division of LBNL, Henry Boateng, Kenzaburo Nagahama, and Kristen Dawson for insightful conversations.

REFERENCES

- [1] N. AILON AND B. CHAZELLE, *Approximate Nearest Neighbors and the Fast Johnson-Lindenstrauss Transform*, in Proceedings of the thirty-eighth annual ACM symposium on Theory of Computing (STOC), Portsmouth, Virginia, May 2006, pp. 557–563.
- [2] H. AVRON AND S. TOLEDO, *Randomized algorithms for estimating the trace of an implicit symmetric positive semi-definite matrix*, Journal of the ACM, 58 (2011).
- [3] S. BAMBERGER, F. KRAHMER, AND R. WARD, *Johnson-lindenstrauss embeddings with kronecker structure*, arXiv preprint arXiv:2106.13349, (2021).
- [4] R. BARRETT, M. BERRY, T. F. CHAN, J. DEMMEL, J. DONATO, J. DONGARRA, V. EIJKHOUT, R. POZO, C. ROMINE, AND H. VAN DER VORST, *Templates for the solution of linear systems: building blocks for iterative methods*, SIAM, 1994.

²<https://github.com/pghysels/STRUMPACK/>

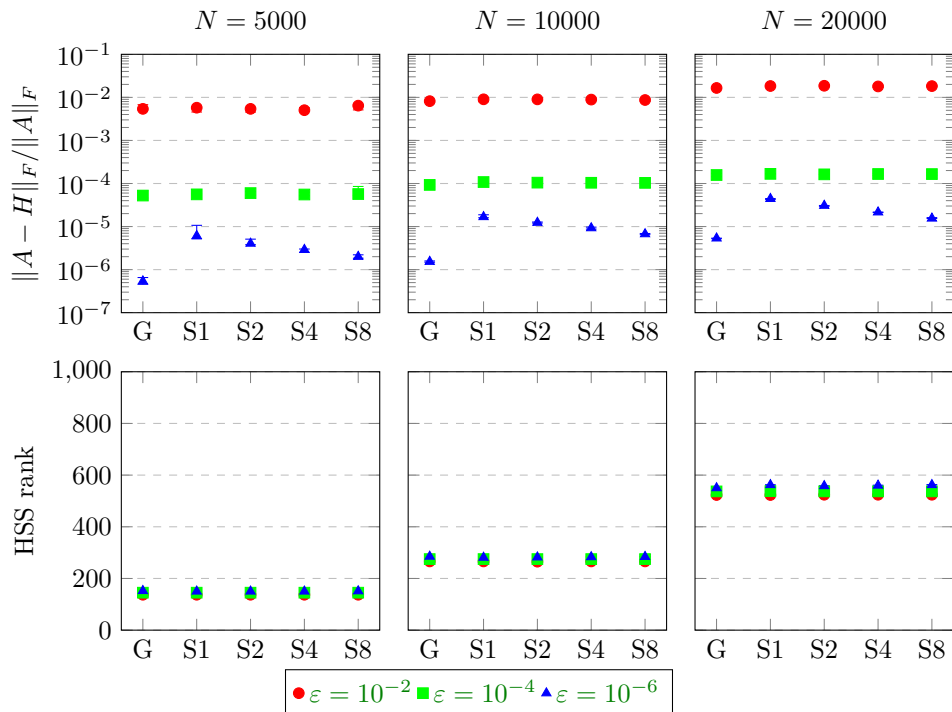


Fig. 6: Scattering wave matrix HSS construction relative error and maximum off-diagonal ranks.

- [5] M. BEBENDORF, *Hierarchical Matrices*, vol. 63 of Lecture Notes in Computational Science and Engineering, Springer, Berlin Heidelberg, 2008.
- [6] S. CHANDRASEKARAN, M. GU, AND W. LYONS, *A fast adaptive solver for hierarchically semiseparable representations*, *Calcolo*, 42 (2005), pp. 171–185.
- [7] S. CHANDRASEKARAN, M. GU, AND T. PALS, *A fast ULV decomposition solver for hierarchically semiseparable representations*, *SIAM Journal on Matrix Analysis and Applications*, 28 (2006), pp. 603–622.
- [8] G. CHÁVEZ, Y. LIU, P. GHYSELS, X. S. LI, AND E. REBROVA, *Scalable and memory-efficient kernel ridge regression*, in 2020 IEEE International Parallel and Distributed Processing Symposium (IPDPS), 2020, pp. 956–965.
- [9] M. B. COHEN, T. JAYRAM, AND J. NELSON, *Simple analyses of the sparse johnson-lindenstrauss transform*, in 1st Symposium on Simplicity in Algorithms (SOSA 2018), Schloss Dagstuhl-Leibniz-Zentrum fuer Informatik, 2018.
- [10] S. DASGUPTA AND A. GUPTA, *An elementary proof of a theorem of johnson and lindenstrauss*, *Random Structures & Algorithms*, 22 (2003), pp. 60–65.
- [11] P. GHYSELS, C. GORMAN, X. LI, AND F.-H. ROUET, *A robust and scalable preconditioner for indefinite systems using hierarchical matrices and randomized sampling*, in IEEE International Parallel and Distributed Processing Symposium (IPDPS), Orlando, USA, May 29 - June 2 2017, IEEE, pp. 897–906.
- [12] G. H. GOLUB AND C. F. VAN LOAN, *Matrix Computations*, Johns Hopkins University Press, Baltimore, fourth ed., 2013.
- [13] C. GORMAN, G. CHÁVEZ, P. GHYSELS, T. MARY, F.-H. ROUET, AND X. S. LI, *Robust and accurate stopping criteria for adaptive randomized sampling in matrix-free hierarchically semiseparable construction*, *SIAM Journal on Scientific Computing*, 41 (2019), pp. S61–S85.
- [14] W. HACKBUSCH, L. GRASEDYCK, AND S. BÖRM, *An introduction to hierarchical matrices*, *Math. Bohem.*, 127 (2002), pp. 229–241.

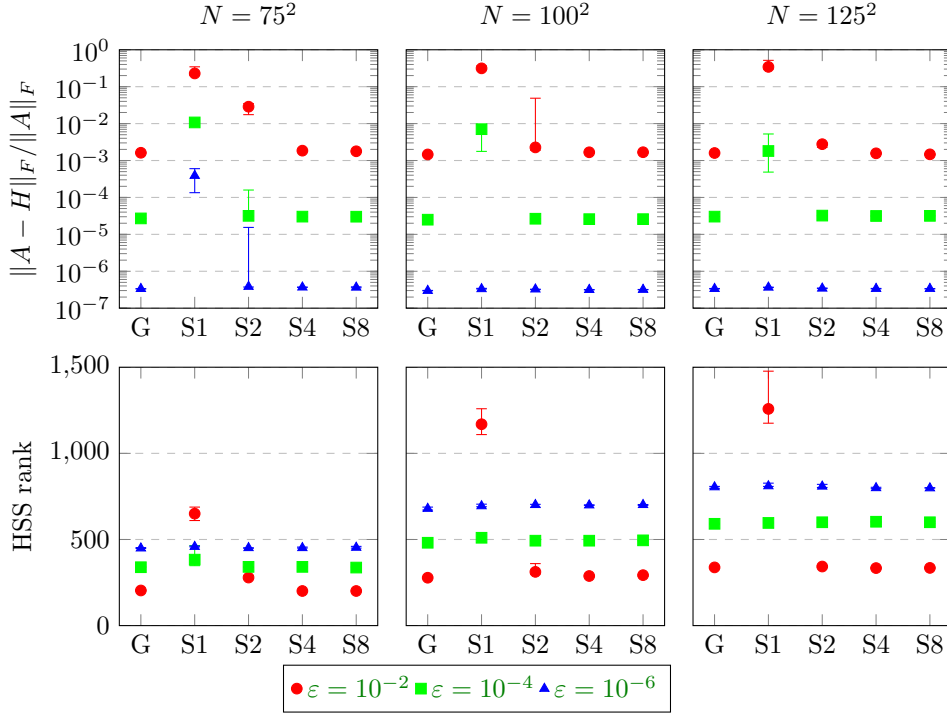


Fig. 7: 3D Poisson frontal matrix HSS construction relative error and maximum off-diagonal ranks.

- [15] W. HACKBUSCH AND B. N. KHOROMSKIJ, *A sparse \mathcal{H} -matrix arithmetic. Part-II: Application to multi-dimensional problems*, Computing, 64 (2000), pp. 21–47.
- [16] N. HALKO, P. MARTINSSON, AND J. TROPP, *Finding structure with randomness: Probabilistic algorithms for constructing approximate matrix decompositions*, SIAM Review, 53 (2011), pp. 217–288.
- [17] W. B. JOHNSON AND J. LINDENSTRAUSS, *Extensions of lipschitz mappings into a hilbert space*, Contemporary mathematics, 26 (1984), p. 28.
- [18] J. R. JONES, F.-H. ROUET, K. V. LAWLER, E. VECHARYNSKI, K. Z. IBRAHIM, S. WILLIAMS, B. ABELN, C. YANG, W. MCCURDY, D. J. HAXTON, ET AL., *An efficient basis set representation for calculating electrons in molecules*, Molecular Physics, 114 (2016), pp. 2014–2028.
- [19] D. KANE AND J. NELSON, *Sparser Johnson-Lindenstrauss Transforms*, Journal of the ACM, 61 (2014).
- [20] J. LEVITT AND P.-G. MARTINSSON, *Linear-complexity black-box randomized compression of hierarchically block separable matrices*, arXiv preprint arXiv:2205.02990, (2022).
- [21] Y. LIU, H. GUO, AND E. MICHIELSEN, *An HSS matrix-inspired butterfly-based direct solver for analyzing scattering from two-dimensional objects*, IEEE Antennas and Wireless Propagation Letters, 16 (2016), pp. 1179–1183.
- [22] P.-G. MARTINSSON, *A fast randomized algorithm for computing a hierarchically semiseparable representation of a matrix*, SIAM Journal on Matrix Analysis and Applications, 32 (2011), pp. 1251–1274.
- [23] P.-G. MARTINSSON AND J. A. TROPP, *Randomized numerical linear algebra: Foundations and algorithms*, Acta Numerica, 29 (2020), p. 403–572.
- [24] J. NELSON AND H. L. NGUYEN, *Osnap: Faster numerical linear algebra algorithms via sparser subspace embeddings*, in 2013 IEEE 54th annual symposium on foundations of computer science, IEEE, 2013, pp. 117–126.
- [25] G. STEWART, *Block Gram-Schmidt orthogonalization*, SIAM Journal on Scientific Computing, 31 (2008), pp. 761–775.

- [26] *STRUMPACK: STRUctured Matrix PACKage*. <http://portal.nersc.gov/project/sparse/strumpack/>.
- [27] J. A. TROPP, *Improved analysis of the subsampled randomized hadamard transform*, *Advances in Adaptive Data Analysis*, 3 (2011), pp. 115–126.
- [28] R. VERSHYNIN, *High-dimensional probability: An introduction with applications in data science*, vol. 47, Cambridge university press, 2018.
- [29] S. WANG, X. S. LI, J. XIA, Y. SITU, AND M. V. DE HOOP, *Efficient scalable algorithms for solving dense linear systems with hierarchically semiseparable structures*, *SIAM Journal on Scientific Computing*, 35 (2013), pp. C519–C544.
- [30] D. P. WOODRUFF, *Sketching as a tool for numerical linear algebra*, *Foundations and Trends® in Theoretical Computer Science*, 10 (2014), pp. 1–157.
- [31] J. XIA, S. CHANDRASEKARAN, M. GU, AND X. S. LI, *Fast algorithms for hierarchically semiseparable matrices*, *Numerical Linear Algebra with Applications*, 17 (2010), pp. 953–976.

Appendix A. Proofs and Other Notes on Theory.

A.1. Proof of Lemma 3.3. We first state the following intermediate lemma to prove Lemma 3.3, following the steps of [30].

LEMMA A.1 (See page 12 of [30]). *Let $x, y \in \mathbb{R}^n$. If $|\|Rz\|^2 - \|z\|^2| \leq \varepsilon$ for all $z \in \{x, y, x + y\}$, then*

$$(A.1) \quad |\langle Rx, Ry \rangle - \langle x, y \rangle| \leq 3\varepsilon \langle x, y \rangle.$$

Proof. The proof follows the argument on page 12 of [30]. Without loss of generality we assume $\|x\| = \|y\| = 1$. Note that

$$(A.2) \quad \begin{aligned} \langle Rx, Ry \rangle &= \frac{1}{2} (\|R(x+y)\|^2 - \|Rx\|^2 - \|Ry\|^2) \\ &= \frac{1}{2} ((1 + \alpha_1)\|x+y\|^2 - (1 + \alpha_2)\|x\|^2 - (1 + \alpha_3)\|y\|^2) \\ &= \frac{1}{2} (2\alpha_1 - \alpha_2 - \alpha_3) + \alpha_1 \langle x, y \rangle. \end{aligned}$$

Since each $|\alpha_i| \leq \varepsilon$, it follows that

$$(A.3) \quad |\langle Rx, Ry \rangle - \langle x, y \rangle| \leq \frac{1}{2} 4\varepsilon + \varepsilon = 3\varepsilon. \quad \square$$

Proof of Lemma 3.3. The proof follows the discussion on pages 12–14 in [30]. It is sufficient to show that the claim holds for $y = Vx$ when y is unit length. Let $\mathcal{S} = \{y \in \text{range}(V) : \|y\| = 1\}$. Furthermore, let \mathcal{N} be a $1/2$ -net for \mathcal{S} . It is possible to choose \mathcal{N} such that $N := |\mathcal{N}| \leq 5^r$ (see Corollary 4.2.13 in [28]). There are $N^2 - N$ sums $x + y$ with distinct $x, y \in \mathcal{N}$. Consequently, the following holds with probability at least $1 - \delta$:

$$(A.4) \quad \left| \|Rx\|^2 - \|x\|^2 \right| \leq \frac{\varepsilon}{12} \quad \text{for all } x \in \mathcal{N} \cup \{y + y' : y, y' \in \mathcal{N}\}.$$

Due to Lemma A.1, the following therefore holds with probability at least $1 - \delta$:

$$(A.5) \quad |\langle Rx, Ry \rangle - \langle x, y \rangle| \leq \frac{\varepsilon}{4} \quad \text{for all } x, y \in \mathcal{N}.$$

Any $y \in \mathcal{S}$ may be represented as

$$(A.6) \quad y = \sum_{i=0}^{\infty} \beta_i y^{(i)},$$

where $|\beta_i| \leq 1/2^i$ and each $y^{(i)} \in \mathcal{N}$. Consequently,

$$(A.7) \quad \begin{aligned} \|Ry\|^2 &= \sum_{i=0}^{\infty} \sum_{j=0}^{\infty} \beta_i \beta_j \langle Ry^{(i)}, Ry^{(j)} \rangle = \sum_{i=0}^{\infty} \sum_{j=0}^{\infty} \beta_i \beta_j (\langle y^{(i)}, y^{(j)} \rangle + \alpha_{i,j}) \\ &= \|y\|^2 + \sum_{i=0}^{\infty} \sum_{j=0}^{\infty} \beta_i \beta_j \alpha_{i,j}, \end{aligned}$$

where each $|\alpha_{i,j}| \leq \varepsilon/4$ due to (A.5). Consequently, we have

$$(A.8) \quad \left| \|Ry\|^2 - \|y\|^2 \right| \leq \sum_{i=0}^{\infty} \sum_{j=0}^{\infty} \frac{1}{2^{i+j}} \frac{\varepsilon}{4} = \varepsilon. \quad \square$$

A.2. Proof of Theorem 3.11. We begin by stating [Lemmas A.2](#) and [A.3](#) which are akin to [Lemmas 3.2](#) and [3.3](#) but with stronger guarantees since they are restricted to SJLT matrices.

LEMMA A.2. *Suppose $R \sim \text{SJLT}(n, d, \alpha)$ with $n > d > \alpha$, and define $\mu = n\alpha/d$. For any $t > 1$, it then holds that*

$$(A.9) \quad \Pr[\|R\|_2^2 \geq t\mu] \leq de^{-\mu} \left(\frac{e}{t}\right)^{t\mu}.$$

In particular, if $t > \max(e^2, \mu^{-1} \log(d/\delta) - 1)$, then

$$(A.10) \quad \Pr[\|R\|^2 \geq t\mu] < \delta.$$

Proof. Recall that we may write R elementwise as in [\(A.20\)](#). Our starting point is the following bound on the two norm:

$$(A.11) \quad \|R\|_2^2 \leq \|R\|_1 \|R\|_\infty = \max_{i \in [d]} \sum_{j=1}^n \eta_{ij},$$

where the inequality is Corollary 2.3.2 in [\[12\]](#), and the equality follows from the standard definitions of the 1- and ∞ -norms (see Section 2.3.2 in [\[12\]](#)). Consequently,

$$(A.12) \quad \begin{aligned} \Pr[\|R\|_2^2 \geq t\mu] &\leq \Pr \left[\max_{i \in [d]} \sum_{j=1}^n \eta_{ij} \geq t\mu \right] = \Pr \left[\bigcup_{i \in [d]} \left\{ \sum_{j=1}^n \eta_{ij} \geq t\mu \right\} \right] \\ &\leq \sum_{i=1}^d \Pr \left[\sum_{j=1}^n \eta_{ij} \geq t\mu \right] = d \Pr \left[\sum_{j=1}^n \eta_{1j} \geq t\mu \right], \end{aligned}$$

where the second inequality follows from subadditivity of measure. Chernoff's inequality (see Theorem 2.3.1 in [\[28\]](#)) gives that

$$(A.13) \quad \Pr \left[\sum_{j=1}^n \eta_{1j} \geq t\mu \right] \leq e^{-\mu} \left(\frac{e}{t}\right)^{t\mu}.$$

Combining [\(A.12\)](#) and [\(A.13\)](#) gives the result in [\(A.9\)](#).

If additionally $t > \max(e^2, \mu^{-1} \log(d/\delta) - 1)$, then the bound in [\(A.9\)](#) simplifies to

$$(A.14) \quad \Pr[\|R\|_2^2 \geq t\mu] \leq de^{-\mu} \left(\frac{e}{t}\right)^{t\mu} \leq de^{-\mu} e^{-t\mu} < \delta. \quad \square$$

The following lemma appeared as Theorem 5 in [\[24\]](#).

LEMMA A.3 (SJLT satisfies subspace embedding property, Theorem 5 from [\[24\]](#)). *Given $R \sim \text{SJLT}(n, d, \alpha)$, $V \in \mathbb{C}^{n \times r}$ and $\varepsilon, \delta \in (0, 1)$. If $\alpha = \Theta(\log^3(r/\delta)/\varepsilon)$ and $d = \Omega(r \log^6(r/\delta)/\varepsilon^2)$ then the following holds with probability at least $1 - \delta$:*

$$(A.15) \quad \left| \|RVx\|^2 - \|Vx\|^2 \right| < \varepsilon \|Vx\|^2 \quad \text{for all } x \in \mathbb{R}^r.$$

We now combine these two results following the steps of [Theorem 3.6](#) to prove a range-finder bound for SJLT matrices.

Proof. We consider the SVD of the matrix A defined in (3.1) and let μ be defined as in Lemma A.2. From Lemma A.2, Lemma A.3 and Remark 3.4 we have that the following two events happen simultaneously with probability at least $1 - \delta$:

$$(A.16) \quad \|R\|^2 \leq \max(e^2\mu, \log(2d/\delta) - \mu), \quad \sigma_{\min}^2(RV_1) \geq 1 - \varepsilon.$$

We proceed under the assumption that the events in (A.16) occur.

Following steps similar to those in the proof of Theorem 3.6, we have

$$(A.17) \quad \|(I - P_Y)A\| \leq \sqrt{\|\Sigma_2\|^2(1 + \|R_2\|^2\|R_1^\dagger\|^2)},$$

where

$$(A.18) \quad \|R_2\|^2 \leq \max(e^2\mu, \log(2d/\delta) - \mu) \quad \text{and} \quad \|R_1^\dagger\|^2 \leq \frac{1}{1 - \varepsilon}.$$

Combining (A.17), (A.18) and the fact that $\|\Sigma_2\| = \sigma_{r+1}(A)$ results in the bound (3.15). \square

A.3. Notes on Theorems 5.2 and 5.3. The results in [2] are concerned with stochastic trace estimation. When A is real, Theorems 5.2 and 5.3 follow directly from Theorems 5.2 and 8.4 in [2] since

$$(A.19) \quad \|AR^T\|_F^2 = \text{trace}(RA^TAR^T) = \sum_{i=1}^d R_i A^T A R_i^T,$$

where R_i is the i th row of R .

When A is complex, we may write it as $A = B + \hat{i}C$ where $B, C \in \mathbb{R}^{m \times n}$. Since the equations in (5.5) then hold and since there is no m -dependence in Theorems 5.2 and 5.3, the result for the complex case follows immediately with no modification to the theorem statements.

A.4. Proof of Theorem 5.4. The proof follows the proof of Theorem 5 in [9] with adaptations made for the matrix case. We first consider the case when A is real. For notational simplicity, let $X = A^T$ and note that $\|AR^T\|_F = \|RX\|_F$. Following the notation in [9], let η_{ij} for $(i, j) \in [d] \times [n]$ be Bernoulli random variables which indicate if the element on position (i, j) of R is nonzero. Moreover, let σ_{ij} for $(i, j) \in [d] \times [n]$ be independent Rademacher random variables taking values in $\{-1, 1\}$ which indicate the sign of the nonzero entries in R . Then, the random matrix R defined elementwise via

$$(A.20) \quad R_{ij} = \eta_{ij}\sigma_{ij}/\sqrt{\alpha}$$

is either a graph or block constructed SJLT depending on how the η_{ij} are drawn. In particular, note that η_{ij} and $\eta_{i'j'}$ are independent for all $i, i' \in [d]$ if $j \neq j'$, but the random variables η_{ij} and $\eta_{i'j}$ are not independent in general.

It is straightforward to show that

$$(A.21) \quad \|RX\|_F^2 - \|X\|_F^2 = \frac{1}{\alpha} \sum_{\ell=1}^m \sum_{i=1}^d \sum_{\substack{j, j'=1 \\ j \neq j'}}^n \eta_{ij}\eta_{i'j'}\sigma_{ij}\sigma_{i'j'}x_{j\ell}x_{j'\ell}.$$

Define the matrices $\tilde{X}^{(i)} \in \mathbb{R}^{n \times m}$ for $i \in [d]$ elementwise via

$$(A.22) \quad \tilde{x}_{j\ell}^{(i)} = \eta_{ij} x_{j\ell}.$$

Let $A_{X,\eta} \in \mathbb{R}^{dn \times dn}$ be block diagonal with the i th $n \times n$ block defined by $\frac{1}{\alpha} (\tilde{X}^{(i)} \tilde{X}^{(i)T})^\circ$, where the function $(\cdot)^\circ$ takes a square matrix as input and returns the same matrix but with the diagonal elements set to zero. Moreover, with a slight overloading of notation, let $\sigma \in \mathbb{R}^{dn}$ denote the vector whose $(j + (i - 1)d)$ th entry is σ_{ij} , i.e.,

$$(A.23) \quad \sigma = [\sigma_{11} \ \cdots \ \sigma_{1n} \ \sigma_{21} \ \cdots \ \sigma_{2n} \ \cdots \ \sigma_{k1} \ \cdots \ \sigma_{kn}]^T.$$

The expression in (A.21) can now be written as the quadratic form

$$(A.24) \quad \|RX\|_F^2 - \|X\|_F^2 = \sigma^T A_{X,\eta} \sigma.$$

For some random variable Y , recall the definition of the \mathcal{L}^q -norm for $1 \leq q \leq \infty$:

$$(A.25) \quad \|Y\|_q = (\mathbb{E}|Y|^q)^{1/q}.$$

We will additionally add superscripts η and σ to denote \mathcal{L}^q -norms and expectations with respect to the variables (η_{ij}) and (σ_{ij}) only, for example

$$(A.26) \quad \|Y\|_{q,\eta} = (\mathbb{E}_\eta |Y|^q)^{1/q}.$$

Henceforth, $q := \lceil 2 \log(1/\delta) \rceil > 1$. Due to independence between the two sets of variables (η_{ij}) and (σ_{ij}) , we have $\mathbb{E}Y = \mathbb{E}_\eta \mathbb{E}_\sigma Y$, and consequently

$$(A.27) \quad \|\sigma^T A_{X,\eta} \sigma\|_q = \|\|\sigma^T A_{X,\eta} \sigma\|_{q,\sigma}\|_{q,\eta}.$$

Applying the Hanson-Wright inequality (Theorem 3 in [9]) to the innermost norm in the expression above followed by the triangle inequality yields

$$(A.28) \quad \|\sigma^T A_{X,\eta} \sigma\|_q \leq C_1 (\sqrt{q} \|\|A_{X,\eta}\|_F\|_{q,\eta} + q \|\|A_{X,\eta}\|\|_{q,\eta}),$$

where C_1 is an absolute constant.

Now, we bound $\|\|A_{X,\eta}\|_F\|_{q,\eta}$. To that end, note that

$$(A.29) \quad \begin{aligned} \|\|A_{X,\eta}\|_F\|_{q,\eta} &= \|\|A_{X,\eta}\|_F^2\|_{q/2,\eta}^{1/2} \\ &\leq \|\|A_{X,\eta}\|_F^2\|_{q,\eta}^{1/2} \\ &= \frac{1}{\alpha} \left\| \sum_{\substack{j,j'=1 \\ j \neq j'}}^n (XX^T)_{jj'}^2 \sum_{i=1}^d \eta_{ij} \eta_{ij'} \right\|_{q,\eta}^{1/2}, \end{aligned}$$

where the inequality follows from an application of Jensen's inequality, and the last equality uses the fact that $\eta_{ij}^2 = \eta_{ij}$. Applying the triangle inequality gives

$$(A.30) \quad \|\|A_{X,\eta}\|_F\|_{q,\eta} = \frac{1}{\alpha} \left(\sum_{\substack{j,j'=1 \\ j \neq j'}}^n (XX^T)_{jj'}^2 \left\| \sum_{i=1}^d \eta_{ij} \eta_{ij'} \right\|_{q,\eta} \right)^{1/2}.$$

Since $q \geq 1$ is an integer, and since $\eta_{ij}^2 = \eta_{ij}$, we can write

$$(A.31) \quad \left(\sum_{i=1}^d \eta_{ij} \eta_{ij'} \right)^q = \sum_{S \in \mathcal{S}} \prod_{(i,j) \in S} \eta_{ij}$$

for some appropriate set \mathcal{S} of subsets of $[k] \times [n]$ (i.e., each $S \in \mathcal{S}$ satisfies $S \subset [d] \times [n]$). One property of both the graph and block constructions of SJLT is that

$$(A.32) \quad \mathbb{E} \prod_{(i,j) \in S} \eta_{ij} \leq \prod_{(i,j) \in S} \mathbb{E} \eta_{ij} = (\alpha/d)^{|S|}$$

for any $S \subset [d] \times [n]$; see the discussion in Section 2 of [9] for details. For $(i, j) \in [d] \times [n]$, let $\tilde{\eta}_{ij}$ be *independent* Bernoulli random variables with $\mathbb{E} \tilde{\eta}_{ij} = \mathbb{E} \eta_{ij} = \alpha/d$. Then, since $\mathbb{E} \prod_{(i,j) \in S} \tilde{\eta}_{ij} = (\alpha/d)^{|S|}$, it follows that

$$(A.33) \quad \mathbb{E} \prod_{(i,j) \in S} \eta_{ij} \leq \mathbb{E} \prod_{(i,j) \in S} \tilde{\eta}_{ij}.$$

Combining this with (A.31) gives

$$(A.34) \quad \left\| \sum_{i=1}^d \eta_{ij} \eta_{ij'} \right\|_{q,\eta} \leq \left\| \sum_{i=1}^d \tilde{\eta}_{ij} \tilde{\eta}_{ij'} \right\|_{q,\eta}.$$

Note that for $j \neq j'$ it holds that $\mathbb{P}(\tilde{\eta}_{ij} \tilde{\eta}_{ij'} = 1) = (\alpha/d)^2$ due to independence. Therefore, $\sum_{i=1}^d \tilde{\eta}_{ij} \tilde{\eta}_{ij'}$ follows a Binomial($d, (\alpha/d)^2$) distribution. It follows from Lemma 2³ in [9] that

$$(A.35) \quad \left\| \sum_{i=1}^d \tilde{\eta}_{ij} \tilde{\eta}_{ij'} \right\|_q \leq C_2 \frac{\alpha^2}{k},$$

where C_2 is an absolute constant. Combining (A.30), (A.34) and (A.35) now gives

$$(A.36) \quad \left\| \|A_{X,\eta}\|_F \right\|_{q,\eta} \leq \sqrt{\frac{C_2}{k}} \|X\|_F^2.$$

Next, we bound $\|A_{X,\eta}\|$. Since $A_{X,\eta}$ is block-diagonal, its two norm is equal to the maximum two norm of its sub-blocks: $\|A_{X,\eta}\| = \max_{i \in [d]} \left\| \frac{1}{\alpha} (\tilde{X}^{(i)} \tilde{X}^{(i)T})^\circ \right\|$. We have

$$(A.37) \quad \begin{aligned} \left\| (\tilde{X}^{(i)} \tilde{X}^{(i)T})^\circ \right\| &= \left\| \tilde{X}^{(i)} \tilde{X}^{(i)T} - \text{diag} \left(\left(\sum_{\ell=1}^m \eta_{ij} x_{j\ell}^2 \right)_j \right) \right\| \\ &\leq \max \left\{ \left\| \tilde{X}^{(i)} \tilde{X}^{(i)T} \right\|, \left\| \text{diag} \left(\left(\sum_{\ell=1}^m \eta_{ij} x_{j\ell}^2 \right)_j \right) \right\| \right\} \\ &\leq \|X\|_F^2, \end{aligned}$$

³In the notation of [9], the condition $B < e$ in the lemma is satisfied if $C_k > 4/e$. Our absolute constant C_d is chosen so that it satisfies this.

where the first inequality is due to the fact that both $\tilde{X}^{(i)}\tilde{X}^{(i)T}$ and $\text{diag}((\sum_{\ell} \eta_{i\ell} x_{j\ell}^2)_j)$ are positive semi-definite. It follows that

$$(A.38) \quad \|A_{X,\eta}\| \leq \frac{1}{\alpha} \|X\|_F^2.$$

Inserting (A.36) and (A.38) into (A.28), and inserting the values of q , d and α gives

$$(A.39) \quad \|\sigma^T A_{X,\eta} \sigma\|_q \leq \varepsilon C_1 \left(2\sqrt{\frac{C_2}{C_d}} + \frac{4}{C_d} \right) \|X\|_F^2.$$

Finally, note that

$$(A.40) \quad \begin{aligned} \mathbb{P}(|\|RX\|_F^2 - \|X\|_F^2| > \varepsilon \|X\|_F^2) &= \mathbb{P}(|\sigma^T A_{X,\eta} \sigma| > \varepsilon \|X\|_F^2) \\ &\leq \varepsilon^{-q} \|X\|_F^{-2q} \|\sigma^T A_{X,\eta} \sigma\|_q^q \\ &\leq \delta, \end{aligned}$$

where the first equality follows from (A.24), the first inequality is Markov's inequality, and the second inequality holds with an appropriate choice⁴ of C_d .

This completes the proof for the case when A is real. Since there is no m -dependence in Theorem 5.4, the case when A is complex follows directly using the argument in Appendix A.3.

Appendix B. Additional Experimental Results. Table 4 shows the final d selected for each method after adaptivity and the HSS rank, the rank of the largest off diagonal block as computed by the interpolative decomposition in the construction. Ideally, the difference between d and the HSS rank should be less than $\Delta d = 64$ in our case meaning that the perfect amount of adaptive steps was taken. We observe that using Gaussian sketching operators and SJLT matrices with $\alpha = 2, 4$ or 8 results in similar adaptive d and HSS rank. When using SJLT matrices with $\alpha = 1$ the number of adaptive steps may be higher because the SJLT matrix is too sparse so new data about the original matrix is learned very slowly, requiring many more adaptive steps.

⁴If C_d is chosen so that $C_1(2\sqrt{C_2/C_d} + 4/C_d) < 1/\sqrt{\varepsilon}$ is satisfied, then second line in (A.40) is less than $1/e^{\log(1/\delta)} = \delta$. Since C_1 and C_2 are absolute constants, the absolute constant C_d can be chosen so that it satisfies this requirement.

Matrix	ϵ_{rel}	n	Final d					HSS rank				
			G	S(1)	S(2)	S(4)	S(8)	G	S(1)	S(2)	S(4)	S(8)
Cov.	10^{-2}	10^3	128	128	128	128	128	97	102	96	97	97
		20^3	256	256	256	256	256	180	179	175	167	159
		30^3	384	384	320	384	384	247	253	221	248	235
	10^{-4}	10^3	192	128	192	192	192	152	154	152	151	152
		20^3	832	896	832	896	832	597	617	586	604	589
		30^3	1984	2176	2112	2112	2112	1472	1530	1520	1511	1470
	10^{-6}	10^3	320	192	256	320	320	226	213	218	222	225
		20^3	1088	1216	1216	1216	1280	835	875	858	863	864
		30^3	2816	2880	2880	2880	2880	2128	2072	2079	2047	2073
QChem Toeplitz	10^{-2}	10K	128	128	128	128	128	11	10	10	10	11
		20K	128	128	128	128	128	13	13	12	12	11
		40K	128	128	128	128	128	12	13	12	12	13
	10^{-4}	10K	128	128	128	128	128	18	20	17	17	16
		20K	128	128	128	128	128	18	19	20	18	20
		40K	128	128	128	128	128	21	28	23	23	21
	10^{-6}	10K	128	128	128	128	128	25	27	24	25	24
		20K	128	128	128	128	128	29	31	29	29	29
		40K	128	128	128	128	128	36	40	37	35	35
Scatt. wave	10^{-2}	5K	192	192	192	192	192	137	137	137	137	137
		10K	320	320	320	320	320	266	266	266	266	265
		20K	576	576	576	576	576	523	523	524	523	524
	10^{-4}	5K	192	192	192	192	192	146	147	145	145	144
		10K	320	320	320	320	320	275	275	274	275	275
		20K	640	640	640	640	640	538	538	535	536	538
	10^{-6}	5K	192	192	192	192	192	153	151	149	151	151
		10K	320	320	320	320	320	284	284	281	282	284
		20K	576	640	640	640	640	550	563	558	559	563
3D Poisson front	10^{-2}	75^2	320	704	384	384	320	204	655	272	205	203
		100^2	448	1216	512	448	512	280	1076	332	291	299
		125^2	576	1664	576	576	576	337	1432	335	336	335
	10^{-4}	75^2	448	512	448	448	512	338	352	338	339	342
		100^2	640	640	704	704	704	474	500	495	493	494
		125^2	832	832	896	896	896	589	594	602	602	598
	10^{-6}	75^2	640	640	640	640	640	451	457	453	451	450
		100^2	960	960	1024	1024	1024	672	695	700	702	702
		125^2	1216	1216	1280	1280	1280	804	810	816	798	799

Table 4: Final d (without Δd) and HSS rank for problems in Table 3.

Appendix C. HSS Algorithm Detailed Description.

Here we describe the steps to compress a symmetric HSS matrix A with dimensions $4k \times 4k$ and HSS rank $r \ll k$ represented by a three level HSS tree shown in Figure 8 using Algorithm 1. Assume that R^T has dimensions $4k \times l_1$. Initially, we compute $S = AR^T$ which has dimensions $4k \times l_1$.

We begin at the leaf level of the HSS tree where we can compress nodes one through four in parallel. We will compress the first node, corresponding to the first Hankel row block, whose rows we have highlighted in Figure 9. By symmetry this also corresponds to the columns of the first Hankel column block.

C.1. Compression of a Leaf Node. First, we store the dense diagonal matrix D_1 in our leaf node 1 this is line 9 of the algorithm. Next, since we do not have the matrix A but instead just the sketch $S = AR^T$ we must figure out what the local

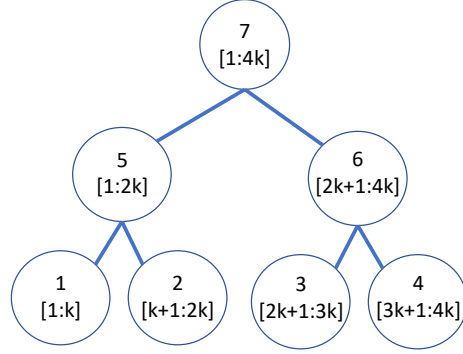


Fig. 8: Three level HSS tree for our compression example with the nodes labeled and the corresponding indices in brackets.

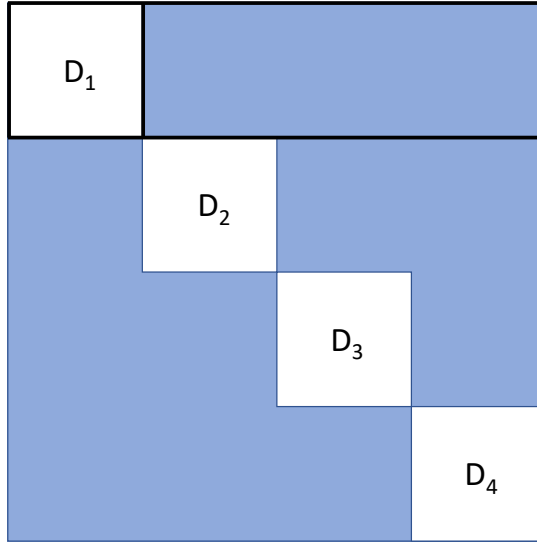


Fig. 9: Leaf level of HSS tree with the first node rows in a box.

sketch of the Hankel row block $H_1 = A(1:k, 1:4k \setminus 1:k) = A(1:k, k+1:4k)$ is (the first k rows excluding the dense diagonal). We compute a sketch of our Hankel row block $S_1^{\text{loc}} = [0, H_1]R^T$ by writing $[0, H_1]R^T = ([D_1, H_1] - [D_1, 0])R^T = (A(1:k, :) - [D_1, 0])R^T = S(1:k, :) - D_1R^T(1:k, :)$ which is line 18 of [Algorithm 1](#).

Next, to compress our approximation of H_1 which is S_1^{loc} with dimensions $k \times l_1$ lines 21-31 of [Algorithm 1](#) verify that S_1^{loc} is a good enough approximation of H_1 . For now, we will assume that it is and skip these lines. Later we will see how if the sketch is not accurate enough, we extend the sketching operator R^T (lines 35-38) by appending columns to it which will require a small modification to the local sketches.

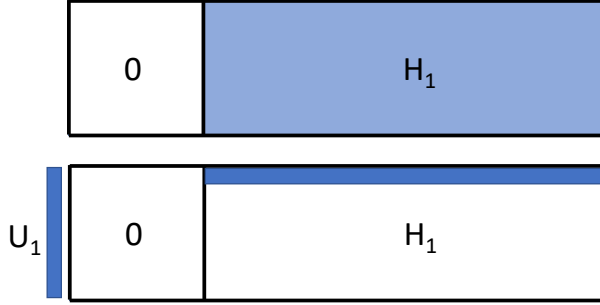


Fig. 10: Compression of the first Hankel block H_1 into U_1 , a basis matrix, and r rows of the original Hankel block, denoted by the thin horizontal stripe (not necessarily the first r rows) and indexed by index set J_1 .

We compute an interpolative decomposition of S_1^{loc} on line 32 of [Algorithm 1](#) such that $S_1^{\text{loc}} \approx U_1 S_1^{\text{loc}}(J_1, :)$ where U_1 has dimensions $k \times r$ and J_1 is a subset of r distinct indices in $[1 : k]$. Then we set the state of node one to compressed (line 33). The interpolative decomposition cleverly gives us a low rank factorization for all of H_1 where U_1 could be thought of as a basis for the Hankel block and J_1 is an index set of rows which define the block. Since $S_1^{\text{loc}} = [0, H_1]R^T \approx U_1 S_1^{\text{loc}}(J_1, :)$ $= U_1 [0, H_1](J_1, :)R^T$ and R^T is full column rank with high probability we have that $[0, H_1] \approx U_1 [0, H_1](J_1, :)$. So we have found a low rank factorization for the Hankel row block which we display in [Figure 10](#).

We can now repeat this process for the rest of the leaf nodes which would result in matrices U_2, U_3, U_4 (dimensions $k \times r$) and index sets J_2, J_3, J_4 (of size r) being computed and stored. For the non-symmetric case we would also compress all of the leaf nodes for the column Hankel blocks as well. We display the result in [Figure 11](#) where we additionally denote the low rank blocks L_1-L_4 which we would like to have compressed.

Remark C.1. The Hankel block does not need to be a contiguous nonzero block, for example $H_2 = [A(k+1 : 2k, 1 : k), 0, A(k+1 : 2k, 2k+1 : 4k)]$ because D_2 is subtracted to compute H_2 .

Next, We show that we have already computed a low rank factorization for L_1-L_4 based on the interpolative decompositions of both the row and column of the two Hankel blocks that intersect at the low rank block. We detail how to compress L_1 in [Figure 12](#). Since we have a row basis for H_1 we can just take the indices of the rows that intersect with L_1 . So we have the factorization $L_1 \approx U_1 A(J_1, k+1 : 2k)$. Similarly, we have basis for the column Hankel block H_2^T which intersected with L_1 because we assumed that our matrix A was symmetric. So the column factorization for L_1 is the conjugate transpose of the row factorization for L_2 which we have already computed, thus $L_1 \approx A(1 : k, J_2)U_2^*$ we can rename U_2^* as V_2 for clarity in the non-symmetric case where the second column Hankel block does not correspond to the conjugate transpose of the second row Hankel block. Combining the row and

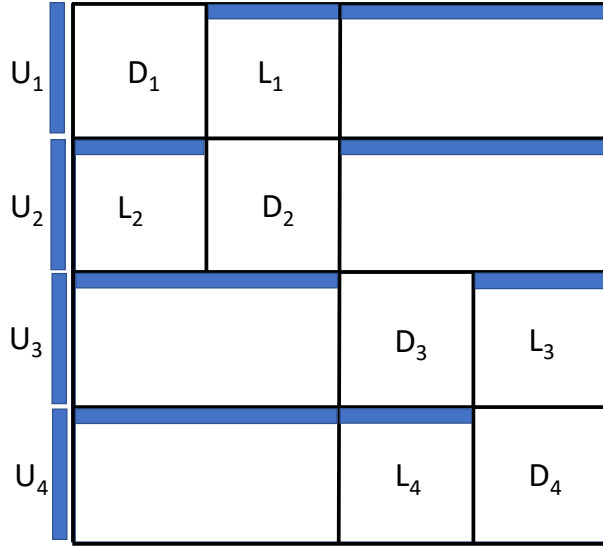


Fig. 11: HSS matrix after all four row leaves have been compressed with the low rank blocks, L_1 – L_4 sections listed .

column factorizations, we have the low rank factorization $L_1 \approx U_1 A(J_1, J_2) U_2^* = U_1 A(J_1, J_2) V_2$. Notice that we currently do not have $A(J_1, J_2)$, the small $r \times r$ matrix of entries of A . This will be queried and stored in the parent node in the next level of the algorithm (line 12 in [Algorithm 1](#)). For completeness we can factorize $L_2 \approx U_2 A(J_2, J_1) U_1^*$, $L_3 \approx U_3 A(J_3, J_4) U_4^*$ and $L_4 \approx U_4 A(J_4, J_3) U_3^*$.

The final step that occurs at each leaf node is to compute R_i^{loc} which corresponds to the sketching operator R^T in the local column basis for the low rank block we have compressed. This will allow us to re-use the computation from our leaf nodes and subtract off the already compressed low rank blocks when trying to compress the parent nodes. Additionally, this allows us to leverage the nested basis property. So for the first leaf node, we compute and store $R_1^{\text{loc}} = U_1^* R^T(1 : k, :)$.

We have completed our compression for the first node, we store five variables: 1. D_1 , 2. U_1 , 3. J_1 which is the dense diagonal block and what we use to represent the Hankel row block for rows $[1 : k]$ and part of the low rank factorization for L_1 and we store 4. S_1^{loc} , 5. R_1^{loc} which we use to represent the sketch for the Hankel row block and the sketching operator for the Hankel row block in the column basis of L_1 which we use for the computation of the parent node.

C.2. Compression of Internal Node. We move on to compressing the second level of the HSS tree whose Hankel row blocks are shown in [Figure 13](#). Before we describe the compression of H_5 , we explain the **nested basis property** which all internal (non-leaf, non-root) nodes in the HSS tree use. This property explains the hierarchical in HSS matrices.

The nested basis property states that for a non-leaf Hankel block, H_5 with children nodes H_1 , H_2 we can write a row (or column) basis U_5^{big} of dimension $2k \times r$ as a

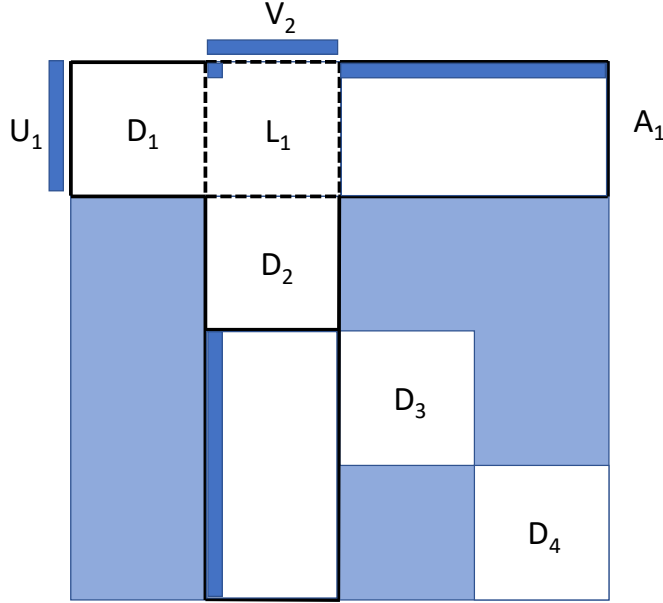


Fig. 12: HSS matrix illustration of how the off diagonal low rank block L_1 is computed and stored.

product of the bases of U_1^{big} , U_2^{big} (dimensions $k \times r$) of H_1 , H_2 respectively and a small matrix U_5 of dimension $2r \times r$:

$$U_5^{\text{big}} = \begin{bmatrix} U_1 & 0 \\ 0 & U_2 \end{bmatrix} U_5.$$

Remark C.2. For leaf node i , $U_i = U_i^{\text{big}}$.

The intuition behind this property is that by constructing a basis U_1^{big} for the first k rows and U_2^{big} for the next k rows, when we want to construct a basis U_5^{big} for the $2k$ rows we should be able to use the basis information from our earlier constructions. When constructing HSS matrices we assume that this property holds.

Now that we have the nested basis property we can explain how this reduces the computation for the compression for node 5 (and any internal node) in [Algorithm 1](#). We would like to have a sketch of H_5 depicted in [Figure 13](#) and compute U_5 , of dimension $2r \times r$. If we consider the matrix $\begin{bmatrix} S_1^{\text{loc}} \\ S_2^{\text{loc}} \end{bmatrix}$ then we have an approximation for the block depicted in the top of [Figure 14](#) because when we computed S_1^{loc} and S_2^{loc} we subtracted the diagonal blocks D_1 and D_2 respectively.

We show how we use the nested basis property and information from the children nodes to compute a local sketch of H_5 . We can subtract our compression of the low dimension blocks L_1 , L_2 which we computed in the children nodes.

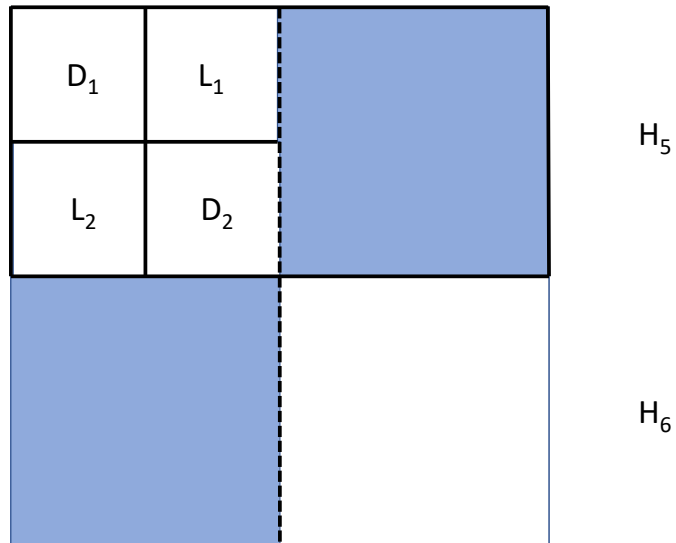


Fig. 13: HSS matrix with the second level of row Hankel blocks highlighted in blue.

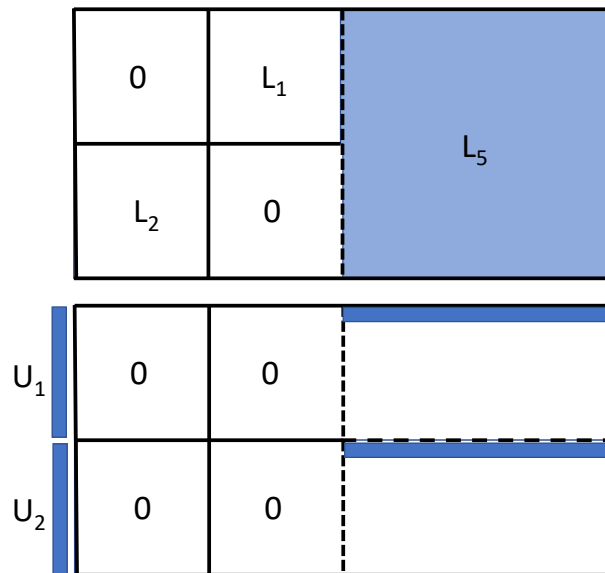


Fig. 14: Node 5 row Hankel block being prepared for compression.

$$\begin{aligned}
S_5 &= \left(\begin{bmatrix} 0 & 0 & H_5(1:k,:) \\ 0 & 0 & H_5(k+1:2k,:) \end{bmatrix} \right) R^T = \left(A(1:2k,:) - \begin{bmatrix} D_1 & L_1 & 0 \\ L_2 & D_2 & 0 \end{bmatrix} \right) R^T \\
&= A(1:2k,:)R^T - \begin{bmatrix} D_1 & L_1 \\ L_2 & D_2 \end{bmatrix} \begin{bmatrix} R^T(1:k,:) \\ R^T(k+1:2k,:) \end{bmatrix} \\
&= \begin{bmatrix} S_1^{\text{loc}} \\ S_2^{\text{loc}} \end{bmatrix} - \begin{bmatrix} 0 & L_1 \\ L_2 & 0 \end{bmatrix} \begin{bmatrix} R^T(1:k,:) \\ R^T(k+1:2k,:) \end{bmatrix} \\
&\approx \begin{bmatrix} U_1^{\text{big}} & 0 \\ 0 & U_2^{\text{big}} \end{bmatrix} \begin{bmatrix} S_1^{\text{loc}}(J_1,:) \\ S_2^{\text{loc}}(J_2,:) \end{bmatrix} - \begin{bmatrix} U_1^{\text{big}}A(J_1, J_2)V_2^{\text{big}}R^T(k+1:2k,:) \\ U_2^{\text{big}}A(J_2, J_1)V_1^{\text{big}}R^T(1:k,:) \end{bmatrix} \\
\text{(C.1)} &= \begin{bmatrix} U_1^{\text{big}} & 0 \\ 0 & U_2^{\text{big}} \end{bmatrix} \left(\begin{bmatrix} S_1^{\text{loc}}(J_1,:) \\ S_2^{\text{loc}}(J_2,:) \end{bmatrix} - \begin{bmatrix} A(J_1, J_2)R_2^{\text{loc}} \\ A(J_2, J_1)R_1^{\text{loc}} \end{bmatrix} \right) \\
&:= \begin{bmatrix} U_1^{\text{big}} & 0 \\ 0 & U_2^{\text{big}} \end{bmatrix} S_5^{\text{loc}}
\end{aligned}$$

Since HSS matrices satisfy the nested basis property to compute a row basis for node 5 we use S_5^{loc} which has dimensions $2r \times l_1$ and contains the nested basis prefactor seen in the second to last row of the above computation which generalizes to any internal HSS tree node. S_5^{loc} corresponds to a sketch of the two dark blue horizontal strips in the bottom of [Figure 14](#) and only requires information already computed in the children nodes.

We go through the steps of compressing H_5 using [Algorithm 1](#). First, since node 5 is the parent node of nodes 1 and 2, it stores the small sub-blocks of A used to compute L_1 and L_2 which in this case is $A(J_1, J_2)$ and $A(J_2, J_1)$, by symmetry only storing the $r \times r$ matrix $A(J_1, J_2)$ is required, line 12 of [Algorithm 1](#). Then on line 20 of [Algorithm 1](#) a local sketch S_5^{loc} as in [\(C.1\)](#) is computed using the sub-blocks of A that we just stored and the information in the children nodes. We then check if the local sketch, S_5^{loc} , is sufficient to approximate H_5 and adaptively increase the size of the sketching operator in lines 21-31 and lines 35-38. We discuss how this adaptation is done in the following section. Assuming that S_5^{loc} is sufficiently accurate, on line 32 of [Algorithm 1](#) we compute our basis U_5 and row indices J_5 in the nested basis defined by U_1 and U_2 . Finally, on line 42 of [Algorithm 1](#) we compute a local sketching operator, R_5^{loc} , in the basis of U_5 which we will use to subtract the block which we have compressed in higher levels of the tree. So we have computed and stored: 1. $A(J_1, J_2)$, 2. S_5^{loc} , 3. U_5 , 4. J_5 , and 5. R_5^{loc} which are the five components that define an internal node.

We can similarly compress H_6 which would now give us all the information to compress L_5 and L_6 by symmetry then move up to the root node.

Remark C.3. When compressing the root node we do not do any compression but instead store the two $r \times r$ blocks of A ($A(J_5, J_6)$ and $A(J_6, J_5)$ here) that are required to compute the low rank factorization for the two largest low rank off diagonal blocks (L_5 and L_6 here).

C.3. Adaptation. At each non-root node of the HSS tree we verify that the sketch of our current node, S_i^{loc} , is sufficiently accurate before we compress it. If S_i^{loc} is sufficiently accurate, which is checked by the computation and stopping criteria on lines 21-31 of [Algorithm 1](#) then we can compress node i , otherwise we increase the size of our global sketching operator and global sketch on lines 35 and 36 (from l_1 to

$l_1 + \Delta d$ in our example). We then mark the state of the current node, i , as partially compressed and restart our compression loop for all of the nodes.

For the compressed nodes we will update their local sketches and sketching operators to have $l_1 + \Delta d$ instead of just l_1 columns. This operation is computed in [Algorithm 1](#) as follows. First on line 14 we set the columns we will be modifying as the final Δd that we added to the global sketch and sketching operator in line 36. Then on lines 18-20 we update the local sketch information, finally on lines 39-42 the local sketching operators are updated.

For the one partially compressed node we will update the sketching operator as for the compressed nodes but we will also check the stopping criteria on lines 27 and 31. If either is met then node i can now be compressed and the algorithm can continue. Otherwise, lines 35-37 will trigger again, expanding the global sketch and sketching operator then marking node j as partially compressed again. Finally, for uncompressed nodes we do not need to update anything, we will use the updated sketching operator and sketches. For a detailed discussion of why we use the stopping criteria on lines 27 and 31 we refer the reader to [section 4](#).